Ore Geology Reviews 157 (2023) 105450

Contents lists available at ScienceDirect

Ore Geology Reviews

journal homepage: www.elsevier.com/locate/oregeorev

Formation of the Huayangchuan (Central China) carbonatite-associated REE-Nb-U polymetallic deposit constrained from monazite mineral chemistry and isotope systematics: HREE enrichment in late-stage monazite

Long-Gang Gao [a], Rui-Zhong Hu [a,b,*], You-Wei Chen [a,*], Xian-Wu Bi [a], Jian-Feng Gao [a], Shao-Hua Dong [a], Jin-Cheng Luo [a]

[a] State Key Laboratory of Ore Deposit Geochemistry, Institute of Geochemistry, Chinese Academy of Sciences, Guiyang 550081, China
[b] College of Earth and Planetary Sciences, University of Chinese Academy of Sciences, Beijing 100049, China

ARTICLE INFO

Keywords:
Carbonatite-related REE-Nb-U deposit
Monazite geochemistry
Huayangchuan
Qinling orogenic belt
HREE mineralization potential

ABSTRACT

The process of enrichment of middle and heavy rare earth elements (MREE and HREE = Sm-Lu plus Y) in magmatic-hydrothermal systems, especially the carbonatite system, remains unclear. Here, we performed in-situ monazite element and isotopic analysis to investigate the genesis of the Huayangchuan REE-Nb-U polymetallic deposit in central China and the enrichment process of MREE and HREE during the evolution of the magmatic hydrothermal system. The Huayangchuan deposit is spatially associated with HREE-rich calcite carbonatites, which exist as two mineralization stages: the ores of the first stage are hosted by carbonatite itself; in the second stage, the ores are present as veins, dominantly by wall rocks around the carbonatite. The results of secondary ion mass spectrometry (SIMS) monazite U-Pb dating on the thin sections yielded Tera-Wasserburg lower intercept ages of 207 ± 4 Ma and 206 ± 5 Ma for carbonatite-hosted monazite and vein-type monazite, respectively. However, some monazite analysis points provide a wide Yanshanian age range (112–182 Ma). The lower intercept age of 206–207 Ma is explained as the mineralization age of the deposit, whereas the wide younger age with higher $^{238}U/^{206}Pb$ and lower $^{208}Pb/^{232}Th$ ratios may be ascribed to the loss of radioactive Pb, as the varying degrees of reworking resulted from the later Yanshanian tectono-thermal event. The monazite laser-ablation multi-collector inductively coupled plasma mass spectrometry (LA-MC-ICPMS) Sr-Nd isotopes from both carbonatite-hosted and wall-rock-hosted vein-type ores indicate that the Huayangchuan deposit is closely related to enriched mantle-derived (EM1) calcite carbonatite but locally affected by late fluid activation. Combined with the integrated age spectra, such reworking processes associated with new weak mineralization widely exist in other carbonatite-related deposits in the Lesser Qinling, but are not important for carbonatite-related mineralization in this area. Controlled by element behaviors, MREE and HREE are more likely to dissolve in hydrothermal fluids, enabling their long-distance migration and deposition, than light REE (LREE) in some carbonatite systems, resulting in much higher MREE and HREE contents of the late monazite in the vein-type ores than those of the early carbonatite-hosted monazite. Therefore, it could be expected that there might be MREE and HREE enrichment and exploration potential in the periphery of some large carbonatite-related LREE-dominated deposits.

1. Introduction

Rare earth elements (REE), as well as niobium (Nb), are important critical resources that are widely used in modern high-tech fields. These critical resources are mostly found in some carbonatites that are widely developed in continental rifts, craton margins, and orogenic belts (Woolley and Kjarsgaard, 2008). Although carbonatite is an important source of REE, the vast majority of carbonatites worldwide are predominantly characterized by light REE (LREE = La, Ce, Pr and Nd) enrichment, rather than middle REE (MREE = Sm to Ho) and heavy REE (HREE = Er to Lu, Y; HREY = HREE + Y) concentration (Henderson, 1984; Woolley and Kjarsgaard, 2008). Recently, with the rapid

* Corresponding authors at: State Key Laboratory of Ore Deposit Geochemistry, Institute of Geochemistry, Chinese Academy of Sciences, Guiyang 550081, China (R.Z. Hu and Y.W. Chen).
E-mail addresses: huruizhong@mail.gyig.ac.cn (R.-Z. Hu), chenyouwei@mail.gyig.ac.cn (Y.-W. Chen).

https://doi.org/10.1016/j.oregeorev.2023.105450
Received 19 December 2022; Received in revised form 18 April 2023; Accepted 18 April 2023
Available online 22 April 2023

development of the high-tech industry, the demand for REE resources, especially MREE and HREE, has increased dramatically, resulting in a sharp rise in their prices (British Geological Survey, 2011). Hence, seeking MREE and HREE remains an important goal for economic geologists worldwide. Available data show that >80% of MREE and HREE resources are produced from HREE-rich ion-adsorption clays in south China (Chi and Tian, 2007; Xie et al., 2016, 2019; Goodenough et al., 2018). With the deepening of exploration, some studies show that a few of LREE-rich carbonatite systems (e.g., Bayan Obo, Tarim, Huayangchuan, Dashigou (China) and Songwe Hill (Malawi)) have shown a certain potential for HREE enrichment (Gong, 1991; Broom-Fendley et al., 2017; Smith et al., 2018; Song et al., 2020; Gao et al., 2021). However, the HREE enrichment process in the LREE-rich carbonatites is still poorly understood, restricting the HREE exploration in the carbonatite-associated systems.

The Qinling orogenic belt (QLOB) is a critical metal-producing area in China (Qiu et al., 1993; Zhang et al., 2019). Among the carbonatites found in China, those of North Qinling are much more specific in that they have not only developed LREE mineralization but also display high HREE contents (Song et al., 2016; Smith et al., 2018; Bai et al., 2019; Gao et al., 2021). The Huayangchuan deposit, located in the Qinling orogenic belt, is a large unique U-Nb-REE polymetallic deposit (Nb:0.11 Mt, 0.02%; REE:0.55 Mt, 0.09%) (Gao et al., 2017). Here, betafite is the main ore of U and Nb. A U content of 93.25% occurs in betafite, compared with 5.72% U in uraninite (Liu et al., 2021). Previous studies have shown that carbonatites are characterized by very high HREE contents in their major minerals (up to 774 ppm in the carbonatitic calcite, Gao et al., 2021), indicating the high potential of HREE mineralization. However, the mechanism of the HREE enrichment in carbonatite-related system is still unclear. These characteristics make the Huayangchuan deposit may as an ideal location to investigate the HREE enrichment process in carbonatite-associated systems.

On the other hand, in terms of the genesis of the Huayangchuan deposit, there are numerous studies of the petrology (Qiu et al., 1993; Xu et al., 2007, 2011; Xue et al., 2020; Gao et al., 2021), metallogenic age (Qiu et al., 1993; Gao et al., 2019; Wang et al., 2020; Xue et al., 2020; Zheng et al., 2020a; Jiang et al., 2020) and metallogenic mechanisms (Xue et al., 2020; Gao et al., 2021) at present. However, the chronology and source of ore-forming materials remain controversial owing to the complexity of the deposit and differences in selected minerals and analysis methods (Gao et al., 2019, 2021; Jiang et al., 2020; Zheng et al., 2020b).

Monazite is a common REE mineral in carbonatite-related REE deposits and is an important ore mineral in the Huayangchuan deposit, which is widely developed, from early to late mineralization stages. Monazite at different stages serves as a record of the entire process of formation and evolution of mineralization; therefore, monazite may as an ideal messenger to uncover the enrichment mechanism of HREE elements in carbonatite-associated systems and clarify the chronology and source of ore-forming materials.

In this study, we conducted detailed in-situ SIMS U-Pb dating, mineral chemical analysis, and LA-MC-ICPMS Sr-Nd isotopic investigations of multi-stage monazites in the deposit. These investigations allow us to (1) accurately constrain the REE-Nb-U metallogenic age, (2) trace ore-forming material sources, (3) summarize carbonatite-related rare polymetallic metallogenic regularities in the Lesser Qinling and additionally (4) help reveal the MREE and HREE migration and enrichment features in some LREE-dominated deposits, which may provide indications for relevant MREE and HREE exploration.

2. Geological setting

The QLOB, located in central China (Fig. 1a), has a long and complex tectonic evolution history. The belt can be divided into the South Qinling (SQL) and North Qinling (NQL) along the Shang-Dan suture (SDS), which was formed owing to the first collision of the SQL and NQL during the Middle Paleozoic (Meng and Zhang, 1999, 2000). The QLOB is an important carbonatite-alkaline complex and an associated critical metal (REE-Nb-U-Mo)-producing zone (Fig. 1b). Many carbonatite complexes are regularly distributed in this belt, such as Huayangchuan, Xigou, Yuantou, Dashigou, Qinlinggou, Dahu, Huangshui'an, Shaxiongdong, Miaoya, Pinghe and Wangjiaping (Fig. 1b, c). Based on the geological distribution features, these carbonatites or carbonatite-alkaline complexes can be divided into the south carbonatite belt (SCB) and the north carbonatite belt (NCB) (Fig. 1b, c; Qiu et al., 1993). The SCB is mainly composed of the Pinghe, Wangjiaping, Miaoya and Shaxiongdong carbonatite complexes, whereas the NCB, located in the Lesser Qinling, is mainly composed of the Xigou, Huayangchuan, Yuantou, Dashigou, Qinlinggou, Dahu and Huangshui'an carbonatite complexes, from west to east (Fig. 1b, c). These carbonatite complexes, including the Huayangchuan carbonatite complexes, are characterized by intruding basement metamorphic rocks of different ages.

The Huayangchuan carbonatite complexes, intruded within the Archean Taihua gneisses and the Paleoproterozoic granitic pegmatite and granite porphyry dykes (Xue et al., 2020), are composed of 500-1000 m wide and ca. 6-km long intrusions with interspersed carbonatite dykes (Fig. 1d) that were subsequently intruded by Mesozoic intermediate-acid magma and were finally overlain by quaternary strata (Fig. 1d).

3. Petrography

The Huayangchuan carbonatite dykes typically comprise a variety of calcite-rich carbonatites, from early quartz-bearing calcite carbonatite, subsequent aegirine-augite calcite carbonatite to late biotite-bearing calcite carbonatite (Fig. 2a-c; Kang et al., 2018). Early quartz-bearing calcite carbonatite (Fig. 2a) is mainly composed of Na-bearing calcite with Na contents from 237 to 390 ppm, and the main rock-forming minerals for aegirine-augite calcite carbonatite (Fig. 2b) are Na-bearing calcite (Na content <167 ppm; Gao et al., 2021) and Na-rich aegirine-augite (Na_2O content up to 8 wt%, unpublished data). Late biotite-bearing calcite carbonatite (Fig. 2c) mainly consists of calcite and minor K-rich minerals, such as biotite and K-feldspar, with intense K-fenitization (dominated by K-feldspar) external to the carbonatite (Fig. 2d). These carbonatite dykes, which are associated with complex mineral assemblages or intense fenitization and biotitization in the late stage (Fig. 2c, 2d), are the predominant U-Nb (betafite) and REE (major allanite-Ce, monazite-Ce, and minor HREE mineral fergusonite-Y (we previously named samarskite-Y)) mineralization bodies. Minor hydrothermal veins of REE-rich minerals (e.g., allanite-Ce and monazite-Ce) are paragenetic with U-Nb-rich betafite, barytocelestite, and apatite (Figs. 2 and 3). Two types of monazites were identified from the ore district: (1) monazite from earlier mineralized carbonatite samples as carbonatite-hosted type (Fig. 2c), and (2) monazite from late hydrothermal vein-type ore that occurs in contact between carbonatite and wall rocks or intrudes into various metamorphic rocks (Fig. 2d, 2e). Carbonatite-hosted monazite mainly occurs in biotite-bearing calcite carbonatite (Figs. 2c, 3a-b) and exhibits an anhedral texture in association with betafite-U-Nb, allanite-Ce, apatite, and calcite (Cal-I-3), with grain sizes ranging from 20 to 150 μm (Fig. 3a-b). Based on the distance from the carbonatite dyke, monazite from vein-type ores can be further subdivided into carbonatite-neared vein-type (Fig. 3c), distant granitic gneiss-hosted vein-type (Fig. 3d), and biotite plagioclase gneiss-hosted vein-type (Fig. 3e). Monazite from carbonatite-neared vein-type ore occurs as long columnar or anhedral granular aggregates or mosaic textures coexisting with betafite-U-Nb, apatite, allanite-Ce, and barytocelestite (Fig. 3c). Monazite from granitic gneiss-hosted vein-type ore coexists with apatite, allanite-Ce, uraninite-U, K-feldspar, and quartz, with grain sizes ranging from 20 to 200 μm (Fig. 3d). In addition to apatite, allanite-Ce, K-feldspar and monazite from biotite plagioclase gneiss-hosted vein-type are also associated with thorite-Th and quartz (Fig. 3e).

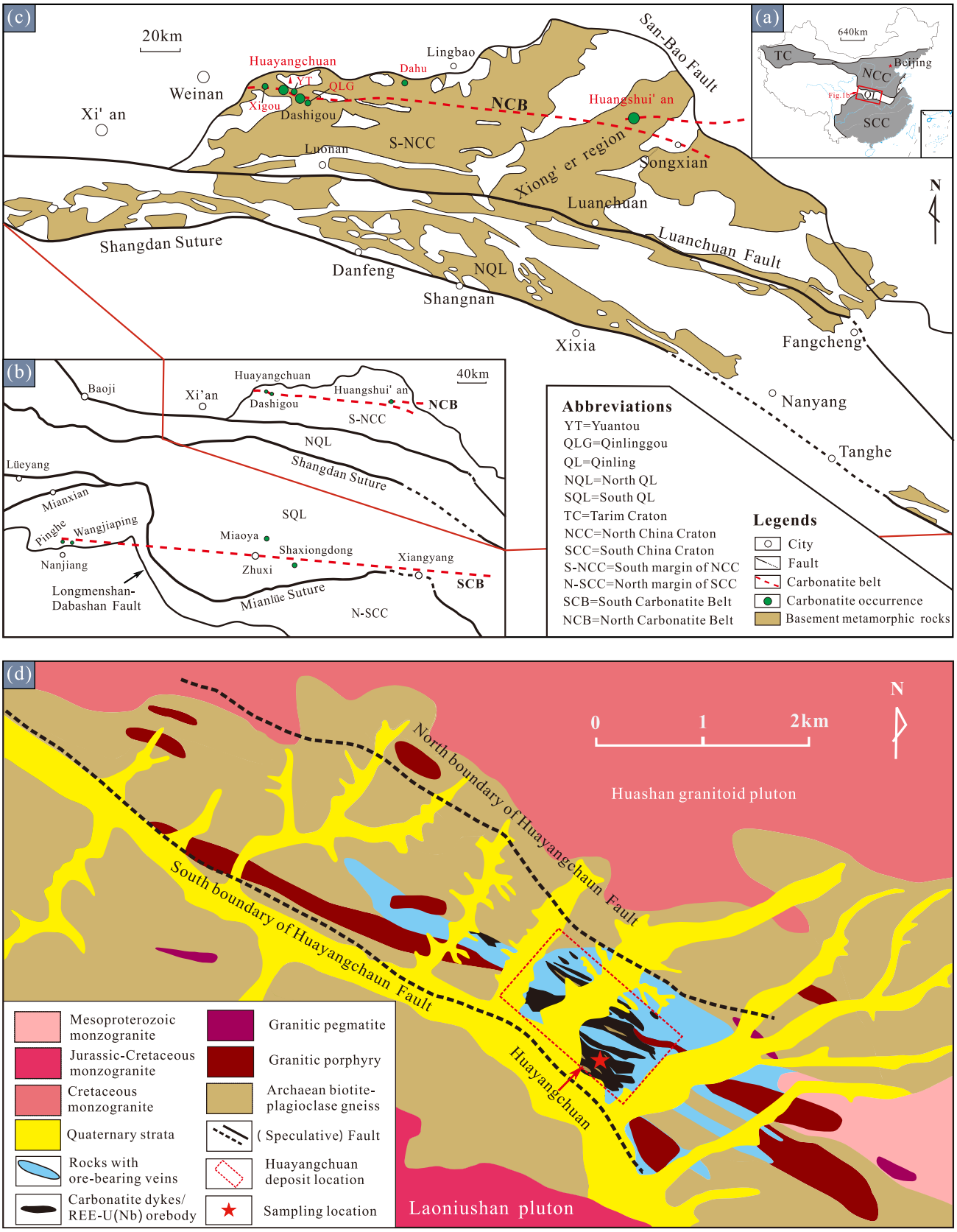

Fig. 1. Geological sketch map of the study area. (a) Tectonic sketch map of China. (b-c) Tectonic sketch map of the Qinling orogenic belt and simplified geological map of the Lesser Qinling (modified from the Geological Atlas of China edited by Ma et al. (2002)). Distribution features of carbonatite-alkaline complexes are based on Qiu et al. (1993). (d) Regional geological map of the Huayangchuan ore district (after Gao et al., 2019; modified from Gao et al., 2017).

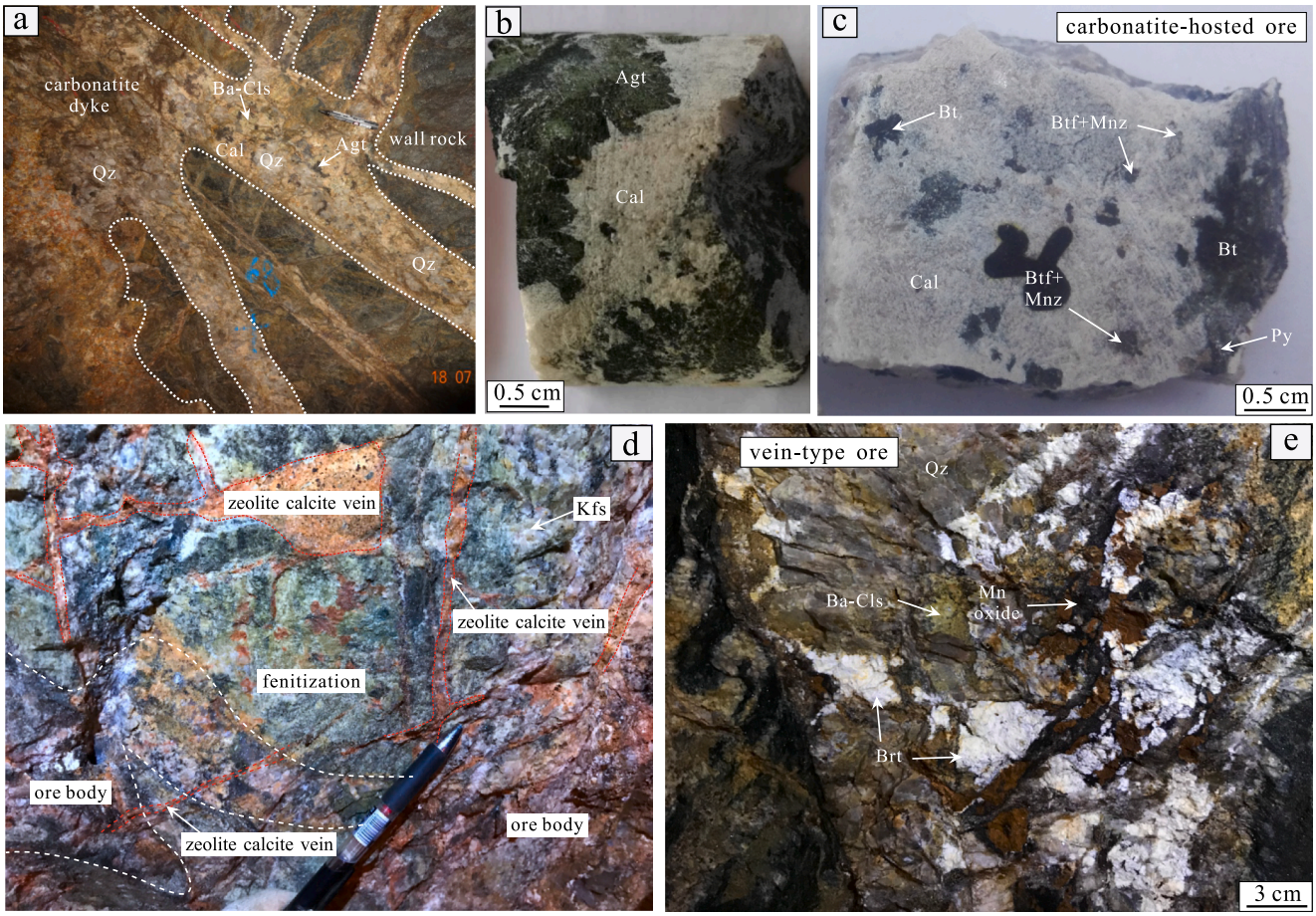

Fig. 2. (a) Occurrence of reticulated carbonatite dyke intruding the biotite-plagioclase gneiss wall rock (Archean Taihua Group) in the Huayangchuan ore district. (b) Aegirine-augite calcite carbonatite. (c) Carbonatite-hosted ore with mineral assemblage of biotite, betafite, monazite, pyrite and carbonatitic calcite. (d) U-Nb-REE ore body and associated fenite cut by latest zeolite calcite veinlets. (e) Late vein-type ore intruded into various metamorphic rocks. Abbreviations: Cal, calcite; Ba-Cls, barytocelestite; Qz, quartz; Agt, aegirine-augite; Btf, betafite; Mnz, monazite; Py, pyrite; Bt, biotite; Kfs, K-feldspar and Brt, barite.

4. Sampling and analytical methods

Two types of REE-Nb-U mineralized samples, namely earlier carbonatite-hosted ore and later vein-type ore, were collected from drillings of the Huayangchuan deposit. REE-Nb-U minerals (monazite and betafite) were identified using a JEOL JSM-7800F field-emission scanning electron microscope, and the monazite in mineralized samples was analyzed via in-situ U-Pb dating, major and trace element analyses, and Sr-Nd isotopic determination.

4.1. In-situ SIMS U-Pb dating of monazite

Individual polished core samples with monazite were collected from primary REE-Nb-U mineralized carbonatites and late hydrothermal vein-type ores in drill holes and prepared for in-situ SIMS U-Pb isotopic analysis.

Polished thin sections were cut from these REE-Nb-U mineralized carbonatites and hydrothermal vein-type ores. Areas of interest were extracted from the polished sections using microdrill. These interesting polished core areas were then assembled along with monazite standards in an epoxy resin and were prepared for Cameca IMS-1280 SIMS U-Pb isotopic analysis at the Institute of Geology and Geophysics, Chinese Academy of Sciences, Beijing. The instrument and analytical methods applied to monazite have been previously described in Li et al. (2013) and Ling et al. (2017). The analysis was conducted using an O_2^- primary beam of approximately 15 × 10 μm on the monazite surface at 10 kV and ca. 0.7nA current. Positive secondary ions were extracted at a potential of 10 kV. The ThO_2^+ signal was used as a reference peak to center the secondary ion beam, energy, and mass adjustments. A standard sample of monazite RW-1 [Th = 11.8 ± 1.0 wt% (2σ), and Th/U = 42.5 ± 3.0 (2σ)] with $^{207}Pb/^{235}U$ age of 904.15 ± 0.26 Ma (2σ) (Ling et al., 2017) was used to calibrate U and Th concentrations and U-Th-Pb isotope ratios. Monazite 44069 was selected as a secondary standard. The Pb/U and Pb/Th ratios, Th concentration, and Th/U ratio were calibrated against the 44069 monazite RM with the recommended U-Pb age of 424.9 ± 0.4 Ma (Aleinikoff et al., 2006). Both common Pb uncorrected U-Pb isotope data and weighted average $^{206}Pb/^{238}U$ age calculations (based on ^{207}Pb-corrected) were performed using ISOPLOT software (Ludwig, 2003).

4.2. In-situ major and trace element compositions

The major element compositions of the monazite grains were analyzed using a JEOL-JAX8230 electron probe microanalysis (EPMA) at the State Key Laboratory of Ore Deposit Geochemistry, Institute of Geochemistry, Chinese Academy of Sciences (SKLODG-IG, CAS), with a 25-kV accelerating potential, 10nA beam current, 1 μm beam diameter, and ca. 10 min counting time on 19 different peaks.

Trace element (including REE) compositions of the monazite were analyzed using laser ablation ICP-MS (LA-ICPMS) with a Coherent GeoLas MV 193 nm laser ablation system connected with an Agilent 7700x ICP mass spectrometer. Spot analyses of monazite were performed with replicate analyses of the reference material NIST SRM 610 to correct for instrumental drift and to use it as an external standard. The

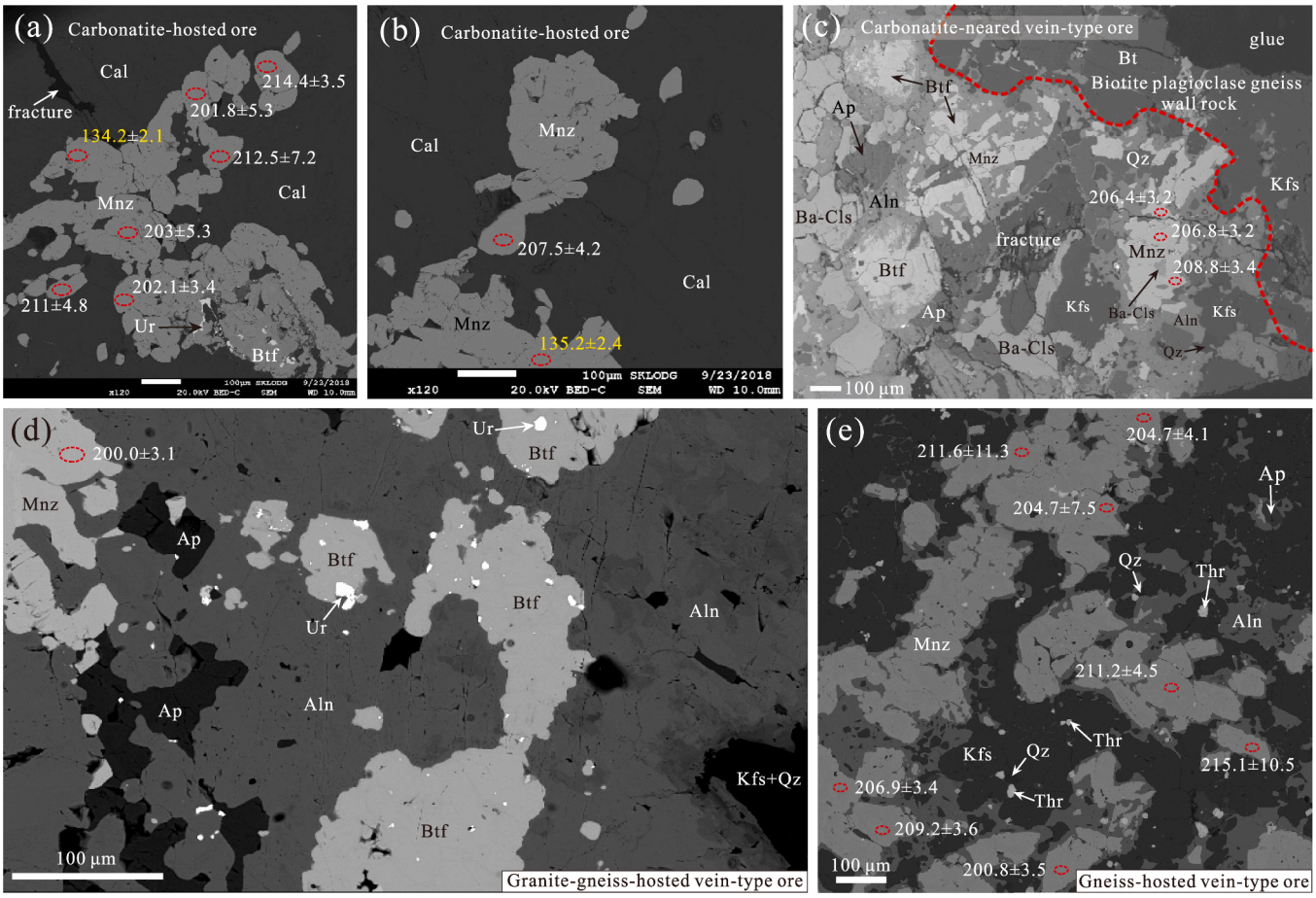

Fig. 3. Backscattered electron (BSE) images showing the features of main U-Nb-REE mineral assemblages in the Huayangchuan deposit. The ellipse-shaped area within the dashed outline includes the sites analyzed using secondary ion mass spectrometry (SIMS), with a series of annotated ^{207}Pb-corrected ^{206}Pb/^{238}U ages (in Ma) with 1σ errors. (a-b) Monazite from carbonatite-hosted ore coexists with betafite, uraninite and fine-grained carbonatitic calcite (Cal-I-3). (c) Carbonatite-neared vein-type ore with mineral assemblage of monazite, betafite, apatite, allanite and barytocelestite. (d) Monazite in granite-gneiss-hosted vein-type ore coexists with betafite, allanite, apatite, uraninite, K-feldspar and quartz. (e) Gneiss-hosted vein-type ore with mineral paragenesis of monazite, allanite, apatite, thorite, quartz, and K-feldspar. Abbreviations: Cal, calcite; Mnz, monazite; Btf, betafite; Ur, uraninite; Ba-Cls, barytocelestite; Qz, quartz; Ap, apatite; Bt, biotite; Kfs, K-feldspar; Aln, allanite; Thr, thorite.

Ce content of monazite determined by EPMA was used as the internal standard calibration.

4.3. In-situ Sr-Nd isotopic analyses

In-situ LA-MC-ICPMS monazite Sr-Nd isotope measurements were conducted on a Nu Plasma III MC-ICP-MS (Nu Instruments) that was attached to a RESOlution-155 ArF193-nm laser ablation system (Australian Scientific Instruments) at SKLODG-IG, CAS. Monazite was ablated in a mixture of helium (350 mL/min) and nitrogen (2 mL/min) gases using the following parameters: 30 s baseline time, 40 s ablation time, and 6 J/cm^2 energy density, with 26–60 μm spot size and 6 Hz repetition rate for the Sr isotope, and 26 μm spot size, and 6 Hz repetition rate for the Nd isotope.

The analytical and interference correction protocol for the Sr analysis followed the method described by Ramos et al. (2004) and fully addressed by Gao and Zhou (2013). One apatite standard AP2 every ten samples and an internal standard consisting of a modern-day coral (MC) every five samples were treated as quality controls. The measured ^{87}Sr/^{86}Sr ratio for modern-day coral (MC) was 0.709179 ± 0.000023 (n = 13), which was identical to the recommended value (0.709174 ± 0.000031) (Hodell et al., 1990).

In the Nd analysis, the interference of ^{144}Sm on ^{144}Nd was controlled by the ^{147}Sm intensity, with a natural ^{144}Sm/^{147}Sm ratio of 0.205484 (Isnard et al., 2005). The mass bias factor of Sm was calculated from the measured isotope ratio of ^{147}Sm/^{149}Sm and its true value of 1.08680 (Isnard et al., 2005). The mass bias of ^{143}Nd/^{144}Nd was normalized to ^{146}Nd/^{144}Nd = 0.7129 with an exponential law. One apatite standard (Durango) every ten samples and the other apatite standard (AP2) for every five unknown samples were treated as quality controls. The measured ^{143}Nd/^{144}Nd ratio for apatite standard AP2 was 0.510997 ± 0.000031 (n = 12), which is identical to the recommended value (AP2: 0.511007 ± 0.000030) (Yang et al., 2014).

5. Results

5.1. SIMS U-Pb dating of monazite

The SIMS U-Th-Pb isotopic ratios and contents of the monazite from the Huayangchuan deposit are presented in Fig. 4 and Table 1. The SIMS monazite U-Pb isotopic results were plotted on Tera-Wasserburg diagrams, yielding well-defined lower-intercept ages of 207.4 ± 4.3 Ma (1σ, n = 32, MSWD = 2.5; Fig. 4a) and 206.1 ± 4.9 Ma (1σ, n = 17, MSWD = 2.4; Fig. 4b), for the carbonatite-hosted ores and the gneiss-hosted hydrothermal vein-type ores, respectively. These lower-intercept ages are similar to the corresponding ^{207}Pb-corrected weighted average ^{206}Pb/^{238}U ages of 209.2 ± 2.9 Ma (1σ, n = 32, MSWD = 0.52; Fig. 4a) and 207.2 ± 4.3 Ma (1σ, n = 12, MSWD = 0.53;

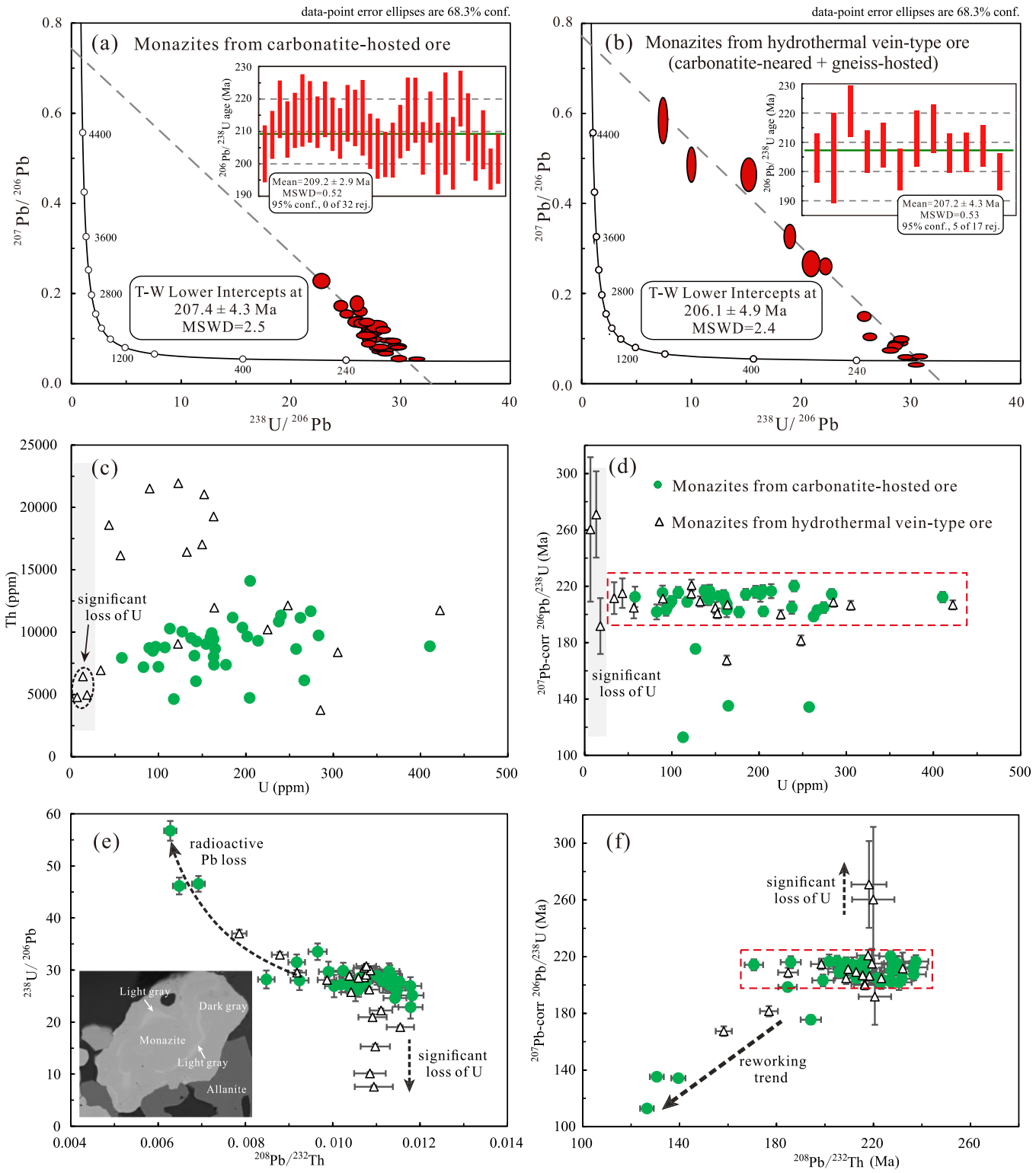

Fig. 4. Tera-Wasserburg (T-W) concordia diagrams of monazite grains from (a) carbonatite-hosted monazite-betafite-allanite ore and (b) later hydrothermal vein-type ore. (c) Scatter plot of U vs. Th abundances of monazites from the carbonatite-hosted ore and vein-type ore indicates significant U loss at some analysis points with low U contents. (d) Plot of U vs. ^{207}Pb-corrected ^{206}Pb/^{238}U age illustrating the influence of U loss. (e) ^{208}Pb/^{232}Th ratio vs. ^{238}U/^{206}Pb ratio diagram, with a monazite grain from carbonatite-hosted ore displaying compositionally heterogeneous feature in the BSE image. (f) ^{208}Pb/^{232}Th age (Ma) vs. ^{207}Pb-corrected ^{206}Pb/^{238}U age (Ma) diagram. Data sources are listed in Table 1.

Fig. 4b) for the carbonite-hosted and vein-type ores, respectively. In addition, part-dashed ellipse-outline SIMS analytical sites with a series of annotated ^{207}Pb-corrected ^{206}Pb/^{238}U ages (in Ma) with 1σ errors are presented in Fig. 3. Based on the mineral paragenesis of monazite-(Ce), betafite-(U-Nb), and allanite-(Ce) (Fig. 3a-d), 206–207 Ma can represent the REE-Nb-U-mineraliztion age and the formation of carbonatite at Huayangchuan. In addition, ^{207}Pb-corrected ^{206}Pb/^{238}U ages show that most monazite data range from 200 to 217 Ma, but a few ages of

Table 1
In-situ SIMS U-Th-Pb dating results of muti-type monazites from the Huayangchuan REE-Nb-U polymetallic deposit.

Ore types	Sample/ spot #	[U] ppm	[Th] ppm	Th/U meas	$^{238}U/^{206}Pb$	±s %	$^{207}Pb/^{206}Pb$	±s %	207-corr age (Ma)	±s %	$^{208}Pb/^{232}Th$	±s %	$^{208}Pb/^{232}Th$	±s %
Carbonatite-hosted type	221-2@02	93	8496	91	29.688	1.92	0.08862	5.64	203.2	4.2	0.00990	2.2	199	4.4
	221-2@03	117	4634	39	29.872	1.53	0.06252	6.92	209.0	3.4	0.01024	2.2	206	4.6
	221-2@04	204	4721	23	28.194	1.76	0.07817	4.43	216.8	3.9	0.01073	2.2	216	4.6
	221-2@05	143	6065	43	27.124	1.52	0.12754	4.98	210.7	4.0	0.01062	2.2	213	4.6
	221-2@06	159	9593	60	28.598	1.70	0.07943	5.43	213.5	3.8	0.01064	2.2	214	4.7
	221-2@07	214	9307	44	26.916	2.14	0.11336	4.51	216.5	5.0	0.01003	2.1	202	4.2
	221-2@09	196	10,362	53	28.007	1.86	0.08590	5.27	216.1	4.2	0.00924	2.2	186	4.2
	221-2@11	155	9041	59	27.704	1.51	0.10484	4.13	212.9	3.6	0.01038	2.1	209	4.5
	221-2@13	137	9526	69	27.218	1.51	0.10421	5.56	216.8	3.8	0.01020	2.2	205	4.4
	221-2@14	411	8859	22	27.392	1.51	0.11516	4.54	212.3	3.7	0.01034	2.1	208	4.4
	221-2@15	100	7216	72	27.658	1.54	0.11784	2.81	209.5	3.6	0.01076	2.3	216	4.9
	221-2@18	107	8762	82	26.903	1.51	0.11665	5.13	215.6	3.9	0.01038	2.2	209	4.6
	221-2@20	185	11,167	60	28.188	1.72	0.08757	4.85	214.2	3.9	0.00848	2.2	171	3.8
	221-2@21	201	9643	48	26.075	2.06	0.14310	5.27	214.2	5.3	0.01052	2.1	212	4.5
	221-2@22	97	8826	91	27.283	1.51	0.13571	4.61	207.0	3.9	0.01056	2.3	212	4.8
	221-2@23	238	10,845	46	26.379	1.52	0.16601	4.18	204.8	4.4	0.01060	2.1	213	4.4
	26-0@06	267	6121	23	29.769	1.54	0.08727	3.71	203.0	3.3	0.01129	2.1	227	4.7
	26-0@07	163	7373	45	27.731	1.54	0.13357	4.99	204.3	4.0	0.01153	2.1	232	4.9
	26-0@11	161	9919	62	27.435	1.55	0.12166	3.96	210.0	3.8	0.01132	2.1	227	4.8
	26-0@13	89	8722	98	24.617	1.66	0.17813	4.31	215.3	5.1	0.01143	2.3	230	5.3
	26-0@14	143	9251	64	25.142	1.58	0.16040	3.61	216.6	4.5	0.01182	2.2	238	5.2
	26-0@15	274	11,665	43	28.907	1.75	0.10213	3.37	204.9	3.8	0.01101	2.1	221	4.7
	26-14@01	283	9729	34	28.676	1.58	0.07381	4.76	214.4	3.5	0.01135	2.1	228	4.7
	26-14@02	83	7190	87	26.077	1.54	0.18343	6.04	201.8	5.3	0.01147	2.3	231	5.2
	26-14@03	58	7936	137	22.861	2.19	0.23281	4.62	212.5	7.2	0.01178	2.3	237	5.5
	26-14@05	163	9434	58	27.867	2.24	0.13343	6.25	203.4	5.3	0.01115	2.1	224	4.8
	26-14@06	240	11,343	47	27.135	1.55	0.09527	5.04	220.1	3.8	0.01130	2.1	227	4.7
	26-14@07	141	8112	58	26.549	1.89	0.14004	4.81	211.4	4.8	0.01142	2.2	230	5.0
	26-14@08	205	14,098	69	29.350	1.56	0.10097	3.85	202.1	3.4	0.01131	2.1	227	4.8
	26-14@10	163	8030	49	26.954	1.67	0.14242	3.96	207.5	4.2	0.01178	2.1	237	5.0
	26-14@11	262	11,142	42	31.497	1.50	0.06177	4.35	198.5	3.0	0.00917	2.1	185	3.8
	26-14@14	177	7380	42	28.429	1.56	0.12539	3.88	201.7	3.7	0.01109	2.2	223	4.9
Mixed ages	221-2@01	127	10,028	79	33.521	1.59	0.10794	4.88	175.5	3.2	0.00965	2.2	194	4.2
	26-14@04	258	8639	34	46.554	1.51	0.06468	5.66	134.2	2.1	0.00692	2.1	139	2.9
	26-14@09	113	10,285	91	56.735	1.89	0.04689	10.29	112.8	2.2	0.00628	2.2	127	2.8
	26-14@12	165	8662	53	46.144	1.62	0.06606	8.24	135.2	2.4	0.00648	2.2	131	2.9
Vein-type	31-3@01	~~13~~	~~6443~~	487	10.142	2.59	0.49118	5.12	~~270.9~~	~~30.6~~	0.01085	3.3	218	7.2
	31-3@03	150	17,038	114	28.873	1.84	0.10363	4.52	204.7	4.1	0.01038	2.2	209	4.6
	31-3@05	56	16,159	287	22.248	1.70	0.27022	4.40	204.7	7.5	0.01111	2.3	223	5.2
	31-3@06	~~34~~	~~6939~~	205	19.024	1.80	0.33519	5.15	~~211.6~~	~~11.3~~	0.01155	2.7	232	6.3
	31-3@08	~~7~~	~~4763~~	716	7.574	3.63	0.58701	5.62	~~260.3~~	~~51.2~~	0.01094	4.0	220	8.7
	31-3@09	123	21,940	179	26.252	1.53	0.11720	4.53	220.7	3.9	0.01084	2.2	218	4.7
	31-3@11	~~18~~	~~4959~~	275	15.315	3.02	0.46934	5.11	~~191.7~~	~~19.8~~	0.01097	3.1	221	6.7
	31-3@12	164	11,960	73	28.604	1.50	0.10271	4.25	206.9	3.4	0.01072	2.1	216	4.6
	31-3@13	132	16,435	124	28.499	1.51	0.09709	6.09	209.2	3.6	0.01059	2.2	213	4.6
	31-3@15	152	21,044	138	29.088	1.56	0.11243	4.04	200.8	3.5	0.01076	2.5	216	5.5
	31-3@16	90	21,520	240	25.741	1.56	0.16156	4.31	211.2	4.5	0.01042	2.2	210	4.6
	31-3@18	~~43~~	~~18,587~~	430	20.948	2.49	0.27597	6.69	~~215.1~~	~~10.5~~	0.01091	3.0	219	6.5
	3-3@02	122	9051	74	28.101	1.68	0.08791	4.48	214.8	3.8	0.00987	2.2	198	4.3
	3-3@03	305	8380	27	29.931	1.50	0.07058	4.55	206.4	3.2	0.01086	2.1	218	4.5
	3-3@05	422	11,757	28	30.436	1.53	0.05649	5.47	206.8	3.2	0.01072	2.2	216	4.8
	3-3@08	285	3744	13	29.500	1.57	0.07293	4.84	208.8	3.4	0.00918	2.2	185	4.1
	5602-C@7	225	10,208	45	30.746	1.50	0.07455	4.88	200.0	3.1	0.01077	2.1	216	4.5
Mixed ages	31-3@14	163	19,273	118	37.020	1.97	0.06979	5.78	167.4	3.4	0.00786	2.1	158	3.3
	5602-B@6	248	12,142	49	32.946	1.50	0.09603	9.79	181.5	3.6	0.00879	2.1	177	3.7

Note: The strikeout data are not included in weighted mean $^{206}Pb/^{238}U$ age (Ma) calculations owing to their low U abundances, and thus large errors in isotopic ratio and $^{206}Pb/^{238}U$ age. The mixed ages are not included in age calculations owing to varying levels of Pb loss.

analytical points range from 112 to 182 Ma (Table 1). Scatter plots of U versus Th abundances and U versus $^{206}Pb/^{238}U$ ages of these monazite dating grains from the carbonatite-hosted ore and vein-type ore are displayed in Fig. 4c-d. In primary carbonatite-hosted ore, the U and Th contents of monazite dating grains are between 58 and 411 ppm and 4634–14098 ppm, respectively, and the composition distribution is relatively concentrated (Fig. 4c). In the late vein-type ore, the ranges of U and Th contents of monazite dating grains were 7–422 ppm and 3744–22940 ppm, respectively and the composition distribution is scattered, with a few low U content (less than 50 ppm) measuring points (Fig. 4c). In the U versus $^{206}Pb/^{238}U$ age diagram, except for a few lower U content (less than 50 ppm) measuring points with relatively wide $^{206}Pb/^{238}U$ age ranges and large errors (not included in the weighted mean $^{206}Pb/^{238}U$ age calculations), most of the other higher U content measuring points have similar age $^{206}Pb/^{238}U$ age ranges (Fig. 4d). Scatter plots of $^{208}Pb/^{232}Th$ ratio versus $^{208}U/^{206}Pb$ ratio and $^{208}Pb/^{232}Th$ ages versus $^{206}Pb/^{238}U$ ages of these monazite dating grains from the carbonatite-hosted and vein-type ores are displayed in Fig. 4e-f.

5.2. Monazite major and trace element compositions

Major and trace element compositions of the monazite are listed in Tables S1 and S2, respectively, and are displayed in Figs. 5, 7, and 8. Primary carbonatite-hosted ore-type monazite [$(La/Yb)_N$ = 14332] contains: SiO_2 (0.16–0.53 wt%), CaO (less than 0.61 wt%), P_2O_5 (27.96–29.58 wt%), ThO_2 (0.22–1.39 wt%), SO_3 (0.12–0.75 wt%), F (0.77–1.03 wt%), La (194315–230781 ppm, average of 209802 ppm, n = 44), Ce (288752–301046 ppm, 293297 ppm), Pr (23134–26581 ppm, 24164 ppm), Nd (59121–77741 ppm, 66878 ppm), Sm (4022–6435 ppm, 4843 ppm), Eu (537–891 ppm, 684 ppm), Gd (1352–2373 ppm, 1702 ppm), Tb (79–135 ppm, 102 ppm), Dy (213–447 ppm, 295 ppm), Y (482–1318 ppm, 807 ppm), Ho (20–66 ppm, 33 ppm), Er (27–135 ppm, 50 ppm), Tm (2–16 ppm, 4 ppm), Yb (5–83 ppm, 14 ppm) and Lu (0.3–9.7 ppm, 1.1 ppm). The contents of monazite from carbonatite-neared vein-type ore is shown to be similar to that of the carbonatite-hosted monazite.

In comparison, late granite-gneiss-hosted vein-type monazite [$(La/Yb)_N$ = 9126] has lower SiO_2 (0.04–0.43 wt%), La (196388–202789 ppm, average of 199653 ppm, n = 10) and SO_3 (0.03–0.53 wt%), and relatively higher concentrations of P_2O_5 (27.96–29.25 wt%), ThO_2 (0.63–1.42 wt%), Pr (25266–26495 ppm, 25758 ppm), Nd (75812–85505 ppm, 80940 ppm), Sm (6458–7279 ppm, 6837 ppm), Eu (1046–1266 ppm, 1158 ppm), Gd (2495–3132 ppm, 2841 ppm), Tb (148–208 ppm, 189 ppm), Dy (373–613 ppm, 529 ppm), Y (982–1934 ppm, 1519 ppm), Ho (34–71 ppm, 58 ppm) and Er (41–101 ppm, 76 ppm) than carbonatite-hosted and carbonatite-neared monazite. Note that biotite-plagioclase gneiss-hosted vein-type monazite [$(La/Yb)_N$ = 9532] has the lowest contents of SiO_2 (<0.37 wt%), SO_3 (0.06–0.81 wt %) and La (155684–184419 ppm, average 168443 ppm, n = 15), and the highest content of HREEs, specifically Gd (range 3560–6460 ppm, average 5073 ppm), Tb (232–521 ppm, 394 ppm), Dy (550–1822 ppm, 1159 ppm), Y (1084–3596 ppm, 2312 ppm), Ho (43–170 ppm, 105 ppm), Er (33–194 ppm, 117 ppm), as well as high levels for most other LREEs, such as Pr (26073–31763 ppm, 28454 ppm), Nd (84292–101534 ppm, 92492 ppm), Sm (8505–13733 ppm, 11110 ppm) and Eu (1315–2375 ppm, 1687 ppm), with the notable exception of Ce (range 273453–298519 ppm, average 286722 ppm).

All types of monazites were shown to have high Th and U contents, but low Ba, Nb, Zr, and Hf contents. In addition, differences were found among monazites from different ore types in the Huayangchuan deposit, with respect to the contents of SiO_2, La_2O_3, SO_3, HREE, ThO_2 and other REE (e.g., Pr, Nd, Sm, and Eu) (Figs. 7 and 8). However, these samples displayed similar REE patterns, which is consistent with the monazite REE pattern in other typical carbonatite-related REE deposits (e.g., Eureka REE deposit, Namibia), but different from that of non-carbonatite-related REE deposits (e.g., Djupedal hydrothermal REE deposit, Sweden) (Fig. 5).

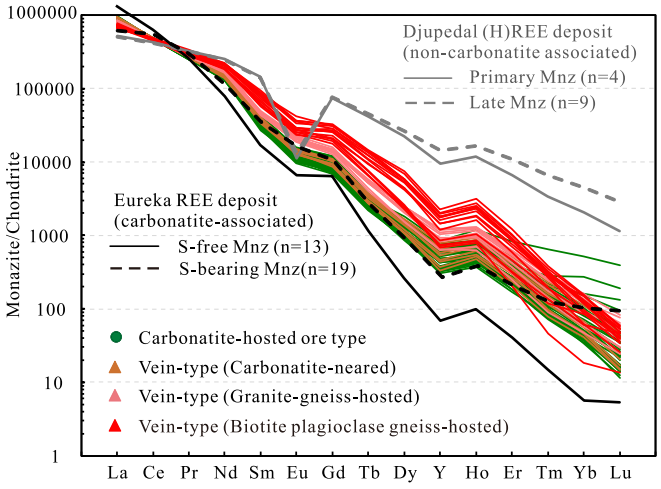

Fig. 5. REE distribution patterns for various monazite types from early carbonatite-hosted type to later vein types. Data sources of the Huayangchuan monazite major and trace elements are listed in Table S2. Normalization values for REE distribution patterns are from McDonough and Sun (1995). Other monazite data sources: Eureka, Broom-Fendley et al. (2019); Djupedal, Andersson et al. (2018). Abbreviations: Mnz, monazite; S, sulfur.

5.3. Monazite Sr-Nd isotopes

The results of in-situ monazite LA-MC-ICPMS Sr-Nd isotopes are listed in Table 2 and presented in Fig. 6. The initial Sr-Nd isotopic values were calculated based on 207 Ma obtained from in-situ monazite SIMS U-Pb ages in this study. The $(^{87}Sr/^{86}Sr)_i$ and $(^{143}Nd/^{144}Nd)_i$ isotopic values for all the monazites range from 0.704851 to 0.706646 and from 0.511730 to 0.512483, respectively.

6. Discussion

6.1. Timing of REE-Nb-U mineralization in the Huayangchuan deposit

Metallogenic chronology has always been an important part of mineral deposit research. However, deposits are often affected by later thermal events and often have multiple ages; therefore, it is difficult to constrain the mineralization age with any precision. Previous chronological studies on the Huayangchuan deposit based on LA-ICP-MS dating of gangue minerals, such as zircon (229 ± 3 Ma, Xue et al., 2020; 1790 ± 15 Ma, Jiang et al., 2020) and titanite (209 ± 3 Ma, Zheng et al., 2020a) gave the Paleoproterozoic and Late Triassic ages. In addition, in-situ electron probe chemical U-Th-Pb dating of uraninite (~201 Ma and ~ 129 Ma, Gao et al., 2019), selected molybdenite Re-Os age (196.8 ± 2.4 Ma, Zheng et al., 2020a) and selected monazite LA-ICPMS U-Pb dating (222.5 ± 6.7 Ma, Wang et al., 2020) yielded Early Cretaceous and Late Triassic ages. The selected monazite dating analysis of the Huayangchuan deposit has been carried out before; however, because of the diversity of ore types and the complexity of tectono-magmatic events from the Archean to Cretaceous in the ore district, a wide range of mineralized ages were obtained—from 129 to 1,800 Ma— thus, the genesis of the deposit remains controversial. One possible reason for this is that some of the dating minerals may have come from wall rocks. Alternatively, they may have been modified to some extent by tectono-magmatic events. In addition, the lack of comparative studies on the metallogenic chronology and isotopic geochemistry of different types of ores is not conducive to understanding deposit genesis.

Field geological work has shown that Indosinian and Yanshanian intermediate-acid magmatism is widely developed around the Huayangchuan ore district (Fig. 1d). This implies that the Huayangchuan deposit is potentially affected by these thermal events. Therefore, minerals with a higher closure temperature are required to better constrain the mineralization age of the deposit. Monazite is one of the principal ore minerals in most carbonatite-related REE deposits, and in the Huayangchuan deposit, it is closely co-existing with U-Nb-REE minerals, such as betafite-U-Nb and allanite-Ce. More importantly, its ultrahigh closure temperature (>900 °C, 10-μm-sized grain, and cooling rate of 10 °C/Ma (Cherniak et al., 2004) makes it suitable for limiting the mineralization age.

In this study, our new monazite SIMS U-Pb data points of primary carbonatite-hosted type ore and late hydrothermal vein-type ore were plotted on a Tera-Wasserburg diagram, yielding well-defined lower-intercept ages of 207.4 ± 4.3 Ma (MSWD = 2.5; Fig. 4a) and 206.1 ± 4.9 Ma (MSWD = 2.4; Fig. 4b), respectively. Meanwhile, these two types of ore samples yielded weighted mean ^{207}Pb-corrected $^{206}Pb/^{238}U$ age of 209.2 ± 2.9 Ma (MSWD = 0.52; Fig. 4a) and 207.2 ± 4.3 Ma (MSWD = 0.53; Fig. 4b), respectively. These chronological data support the conclusion that the REE-Nb-U mineralization in the Huayangchuan deposit formed at 207 ± 4 Ma, which is consistent with our previous age

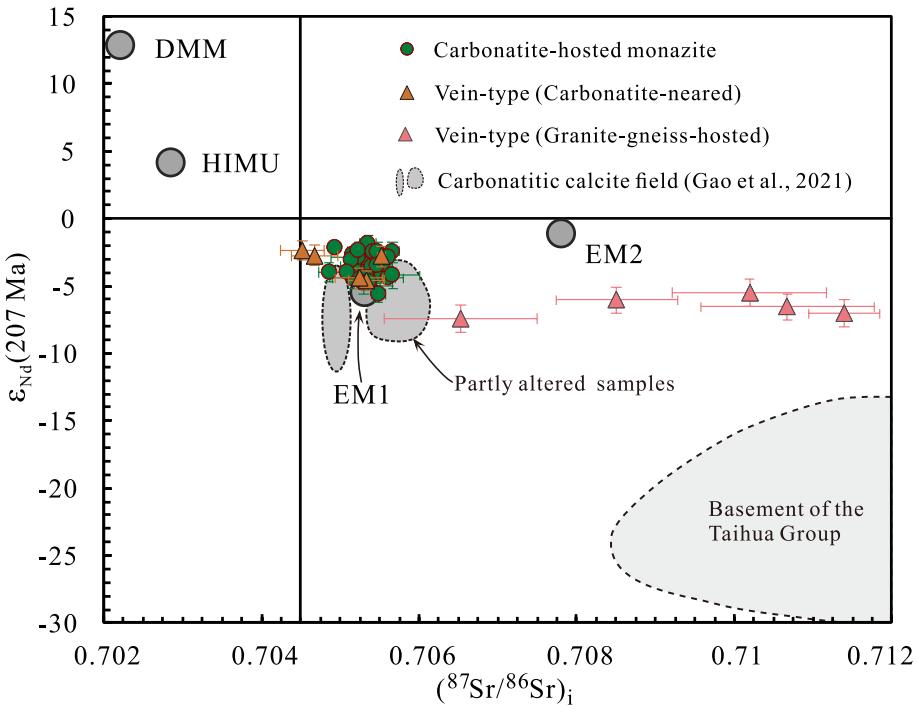

Fig. 6. In-situ Sr–Nd isotopic data for various monazites from ores of early carbonatite-hosted type to later vein types at Huayangchuan in this study. Data sources of the Huayangchuan monazite Sr–Nd isotopes are listed in Table 2. The Sr-Nd isotopic fields of the Huayangchuan carbonatitic calcite and the Taihua Group basements are cited from Gao et al. (2021) and Gao et al. (2014), respectively. The binary diagram and the DMM, EM1, EM2 and HIMU end-member components are taken from Zindler and Hart (1986).

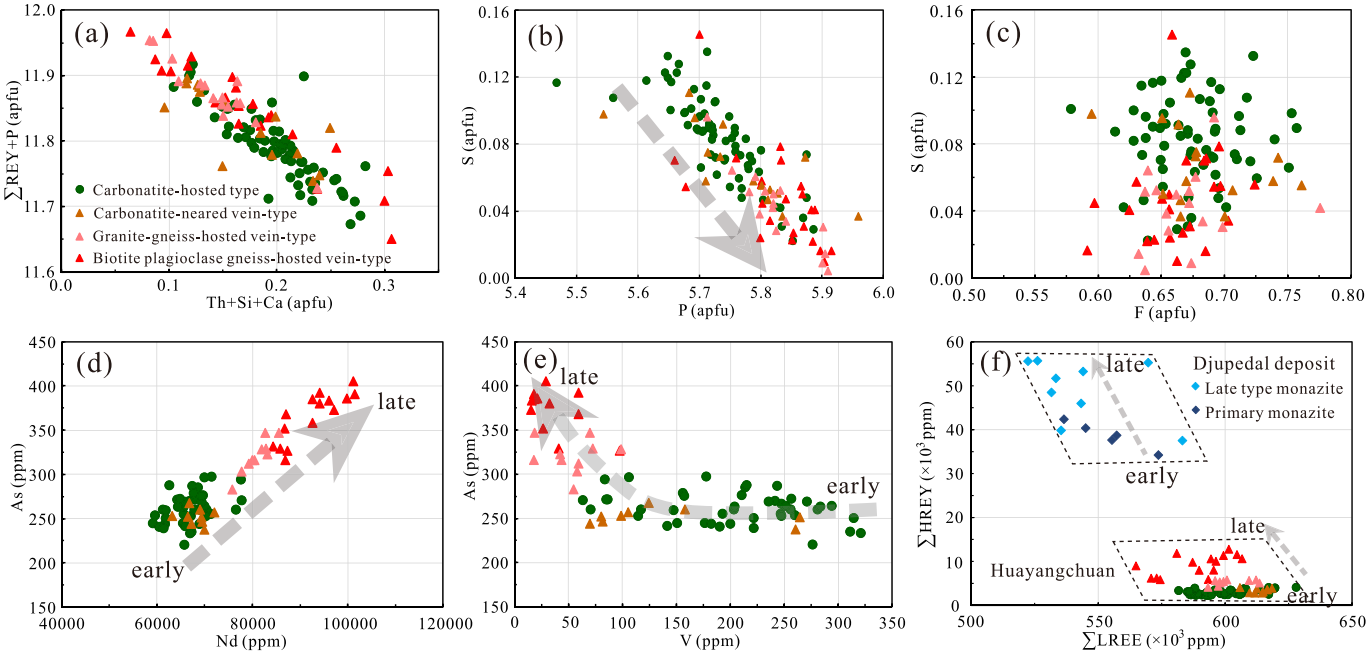

Fig. 7. Correlation diagrams of major and trace elements of various monazite from ores of early carbonatite-hosted type to slightly late vein types at Huayangchuan. Data sources of the Huayangchuan monazite major and trace elements are listed in Table S1 and Table S2. On the ΣLREE vs. ΣHREY (HREY = HREE + Y) diagram, the primary and late-type monazite data of the Djupedal deposit are from Andersson et al. (2018).

(201 ± 3 Ma) obtained from uraninite by electron probe U-Th-Pb chemical dating within analytical errors (Gao et al., 2019). However, it is noteworthy that some single grain monazite ^{207}Pb-corrected ^{206}Pb/^{238}U ages varies from 181.5 ± 3.6 Ma to 112.8 ± 2.2 Ma, with a strongly linear relationship and displays a reworking trend from Indosinian to Yanshanian (Fig. 4f), similar to that reported by Li et al. (2011) from the adjacent Dahu Au-Mo deposit. In particular, two monazite grains yielded concordant ages of 134.2 ± 2.1 Ma (26–14@04) and 135.2 ± 2.4 Ma (26–14@12) (Fig. 3a-b, Table 1), respectively, which coincides with the time of the Early Cretaceous magmatism represented by Huashan granitoid complexes in the region (143 ± 1 to 134 ± 1 Ma; Guo et al., 2009; Zhang et al., 2015). We can only speculate why some monazite grains exhibit a wide age range; prolonged mineralization or disturbance as a result of tectonic thermal events might be the reason.

Regarding prolonged carbonatite magmatism and genetically associated REE-Nb-U mineralization (See discussion in section 6.2), as we know, the features of carbonatite magma—small scale, low density, low viscosity (Dobson et al., 1996) and volatile-rich matter (Keppler,

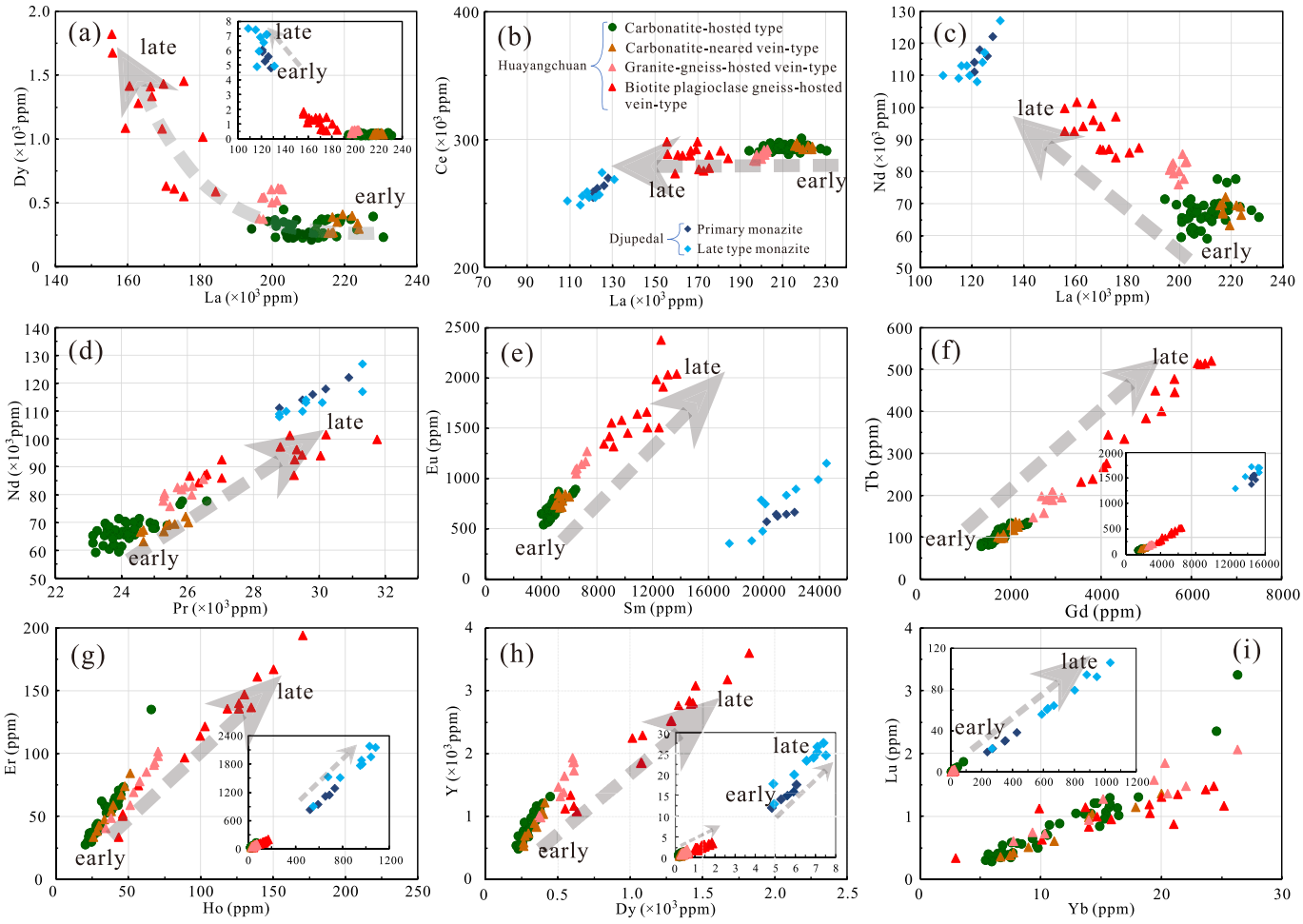

Fig. 8. Correlation diagrams of individual REEs of various monazite from early carbonatite-hosted type to later vein types at Huayangchuan. REE data sources of the Huayangchuan monazite are listed in Table S2. The primary and late-type monazite REE data of the Djupedal deposit are from Andersson et al. (2018).

2003)—enabled it to rise rapidly (20–65 m/s, Genge et al., 1995) to the shallow part of the earth, where it crystallized or erupted to the surface after forming in the source region. Thus, protracted magmatism and associated mineralization are unlikely. As for the possible mechanism of thermal event modification, these so-called Yanshanian monazites are similar to Triassic monazites in terms of morphology, mineral association (Fig. 3), and REE patterns (Fig. 5). Metasomatic experimental studies show that, despite monazite with high closure temperature, it is sensitive to hydrothermal reworking, and fluid-induced alteration can disturb the U-Pb and Th-Pb ages in monazite (Budzyń et al., 2021; Li et al., 2021), especially when fractures and pores are developed. Therefore, the wide age range implies that the Huayangchuan deposit has experienced Yanshanian tectono-hydrothermal event overprinting since its formation, resulting in radioactive Pb loss (Fig. 4e) and/or U loss (Fig. 4c, f) and even systematic resetting for some monazite grains to some extent (Fig. 4e). This proposal is further supported by the similar Nd but higher Sr isotopic compositions of some monazites (Fig. 6) and by our first discovery of the carbonatite-hosted core-rim textural uraninite associated with the Indosinian core (~201 Ma) and Yanshanian rim (~129 Ma) with coupled dissolution and reprecipitation features in the deposit (Gao et al., 2019). In addition, the findings of other case studies from both Huayangchuan (Cai et al., 2020) and the adjacent Dahu Au-Mo deposit (Li et al., 2011) support the existence of such tectono-thermal events. Considering that Yanshanian reworking mineralization exists in the deposit, it is worth investigating whether this mineralization is an important carbonatite-related rare metal metallogenic event in the Lesser Qinling. The results of previous studies have shown that Indosinian betafite is the main ore mineral of U and Nb in the deposit, and only a few new Yanshanian uraninite grains were formed (Gao et al., 2019), but not accompanied by the formation of a large number of new REE minerals around the REE-rich monazite, allanite, or REE-bearing apatite and calcite during the reworking process (Gao et al., 2021). In fact, 93.25% U occurs in betafite, and 5.72% U occurs in uraninite (Liu et al., 2021). Hence, the Huayangchuan REE-Nb-U polymetallic deposit was mainly formed in the Late Triassic (207 ± 4.3 Ma), but locally overprinted by Early Cretaceous magmatism events.

In addition to Huayangchuan, there are many other HREE-rich carbonatite occurrences and/or associated deposits in the NCB of the Lesser Qinling, such as Xigou, Yuantou, Qinlinggou, Dashigou, and Huangshui'an, an area extending nearly 200 km from west to east (Fig. 1c). Based on the work of the Huayangchuan case and previous studies of the Dashigou deposit (Gao, 2019), in combination with geochronological and mineralogical studies on other NCB carbonatites, these HREE-rich carbonatites and associated rare metal deposits were mainly formed during the Late Triassic (Fig. 9; Table S3 and its references) but with weak or negligible Yanshanian reworking mineralization.

6.2. *Source(s) of the ore-forming fluids*

Sr isotopic variations combined with Nd isotopic compositions of whole rock and minerals can be used to trace the origin of magma and ore-forming materials (Wall and Zaitsev, 2004; Cao et al., 2021; Gao et al., 2021). Monazite, an important ore mineral in carbonatite-associated systems, contains high concentrations of Sr (>300 ppm)

Table 2
In-situ LA-MC-ICPMS Sr-Nd isotopic data of the Huayangchuan multi-type monazites.

Ore type	Spot No.	$^{87}Rb/^{86}Sr$	2 Sigma	$^{87}Sr/^{86}Sr$	2 Sigma	$(^{87}Sr/^{86}Sr)_i$	$^{147}Sm/^{144}Nd$	2 Sigma	$^{143}Nd/^{144}Nd$	2 Sigma	$(^{143}Nd/^{144}Nd)_i$	$\varepsilon_{Nd}(207)$	error	T_{DM}(Ga)	T_{2DM}(Ga)
Carbonatite-hosted type (early)	221-2-1	0.000142	0.000044	0.705166	0.000160	0.705166	0.049067	0.000036	0.512304	0.000038	0.512237	−2.62	0.74	0.78	1.20
	221-2-2	0.000215	0.000043	0.705369	0.000140	0.705369	0.048769	0.000110	0.512199	0.000037	0.512133	−4.66	0.72	0.88	1.37
	221-2-3	0.000069	0.000030	0.704934	0.000120	0.704934	0.050537	0.000130	0.512330	0.000080	0.512261	−2.15	1.56	0.77	1.17
	221-2-4	0.000211	0.000049	0.705148	0.000160	0.705148	0.048701	0.000068	0.512280	0.000036	0.512214	−3.07	0.70	0.80	1.24
	221-2-5	0.008829	0.000250	0.705632	0.000220	0.705606	0.047605	0.000030	0.512289	0.000038	0.512224	−2.88	0.74	0.79	1.23
	221-2-6	0.000053	0.000026	0.705221	0.000096	0.705221	0.045823	0.000046	0.512311	0.000038	0.512249	−2.40	0.74	0.76	1.19
	221-2-7	0.000148	0.000041	0.705092	0.000150	0.705091	0.047503	0.000034	0.512232	0.000034	0.512167	−3.99	0.66	0.84	1.32
	26-0-1	0.002453	0.000250	0.705352	0.000450	0.705345	0.045407	0.000019	0.512206	0.000043	0.512145	−4.43	0.84	0.86	1.35
	26-0-2	0.000655	0.000110	0.705669	0.000340	0.705667	0.046986	0.000160	0.512218	0.000048	0.512155	−4.23	0.93	0.85	1.34
	26-0-3	0.000284	0.000073	0.705301	0.000200	0.705300	0.051291	0.000069	0.512194	0.000043	0.512125	−4.82	0.84	0.90	1.38
	26-0-4	0.000313	0.000081	0.705237	0.000360	0.705236	0.045914	0.000065	0.512286	0.000050	0.512224	−2.88	0.97	0.79	1.23
	26-14-1	0.000139	0.000014	0.705483	0.000070	0.705482	0.045073	0.000051	0.512262	0.000037	0.512201	−3.33	0.72	0.80	1.26
	26-14-2	0.000293	0.000038	0.705284	0.000140	0.705283	0.047830	0.000087	0.512276	0.000033	0.512212	−3.12	0.64	0.80	1.25
	26-14-3	0.000353	0.000047	0.705356	0.000100	0.705355	0.046502	0.000065	0.512339	0.000030	0.512276	−1.86	0.58	0.74	1.14
	26-14-4	0.000104	0.000021	0.705176	0.000077	0.705176	0.048046	0.000180	0.512208	0.000036	0.512142	−4.47	0.70	0.87	1.36
	26-14-5	0.000248	0.000022	0.705274	0.000089	0.705273	0.049312	0.000031	0.512242	0.000033	0.512176	−3.83	0.64	0.84	1.30
	26-14-6	0.000208	0.000031	0.705289	0.000110	0.705288	0.049259	0.000042	0.512281	0.000034	0.512214	−3.07	0.66	0.81	1.24
	26-14-7	0.000187	0.000023	0.705470	0.000091	0.705469	0.046514	0.000081	0.512255	0.000035	0.512192	−3.51	0.68	0.82	1.28
	26-14-8	0.000102	0.000023	0.705156	0.000084	0.705155	0.046753	0.000120	0.512273	0.000033	0.512210	−3.16	0.64	0.80	1.25
	26-14-9	0.000180	0.000025	0.705228	0.000110	0.705227	0.049468	0.000046	0.512239	0.000033	0.512172	−3.90	0.64	0.85	1.31
	26-14-10	0.000281	0.000030	0.705430	0.000110	0.705429	0.050617	0.000020	0.512305	0.000036	0.512236	−2.65	0.70	0.79	1.21
	26-14-11	0.000469	0.000021	0.705423	0.000079	0.705421	0.048906	0.000065	0.512309	0.000034	0.512243	−2.51	0.66	0.78	1.20
	26-14-12	0.000167	0.000023	0.705482	0.000087	0.705482	0.048402	0.000025	0.512150	0.000032	0.512084	−5.61	0.62	0.92	1.45
	26-14-13	0.000393	0.000039	0.704861	0.000140	0.704860	0.047135	0.000042	0.512232	0.000035	0.512168	−3.97	0.68	0.84	1.31
	26-14-14	0.000015	0.000024	0.705315	0.000091	0.705315	0.045313	0.000035	0.512216	0.000035	0.512155	−4.24	0.68	0.85	1.34
	26-14-15	0.000130	0.000023	0.705457	0.000092	0.705457	0.048460	0.000078	0.512225	0.000033	0.512160	−4.14	0.64	0.85	1.33
	26-14-16	0.000080	0.000034	0.705397	0.000140	0.705396	0.045251	0.000049	0.512251	0.000035	0.512190	−3.55	0.68	0.81	1.28
	26-14-17	0.000422	0.000039	0.705238	0.000140	0.705237	0.047057	0.000073	0.512310	0.000038	0.512246	−2.45	0.74	0.77	1.19
	26-14-18	0.000314	0.000038	0.705472	0.000140	0.705471	0.047284	0.000060	0.512309	0.000037	0.512245	−2.47	0.72	0.77	1.19
	26-14-19	0.000180	0.000026	0.705611	0.000089	0.705611	0.049799	0.000072	0.512215	0.000033	0.512148	−4.37	0.64	0.87	1.35
	26-14-20	0.000065	0.000023	0.705541	0.000110	0.705541	0.046371	0.000059	0.512262	0.000038	0.512200	−3.36	0.74	0.81	1.27
	26-14-21	0.000482	0.000026	0.705664	0.000092	0.705663	0.038137	0.000098	0.512299	0.000036	0.512248	−2.42	0.70	0.74	1.19
	26-14-22	0.000470	0.000041	0.705176	0.000170	0.705174	0.046800	0.000097	0.512255	0.000041	0.512191	−3.52	0.80	0.82	1.28
	26-14-23	0.000171	0.000032	0.705475	0.000120	0.705474	0.047103	0.000086	0.512258	0.000037	0.512194	−3.47	0.72	0.82	1.27
Carbonatite-neared vein type (late)	3-3-1	0.000168	0.000062	0.705335	0.000220	0.705335	0.050304	0.000052	0.512204	0.000036	0.512136	−4.61	0.70	0.88	1.37
	3-3-2	0.000198	0.000083	0.705239	0.000310	0.705238	0.050915	0.000056	0.512214	0.000037	0.512145	−4.43	0.72	0.88	1.35
	3-3-3	0.000221	0.000073	0.704520	0.000280	0.704519	0.048500	0.000031	0.512317	0.000037	0.512251	−2.36	0.72	0.77	1.18

(*continued on next page*)

Table 2 (*continued*)

Ore type	Spot No.	$^{87}Rb/^{86}Sr$	2 Sigma	$^{87}Sr/^{86}Sr$	2 Sigma	$(^{87}Sr/^{86}Sr)_i$	$^{147}Sm/^{144}Nd$	2 Sigma	$^{143}Nd/^{144}Nd$	2 Sigma	$(^{143}Nd/^{144}Nd)_i$	$\varepsilon_{Nd}(207)$	error	$T_{DM}(Ga)$	$T_{2DM}(Ga)$
	3-3-4	0.039169	0.001300	0.704793	0.000290	0.704678	0.050184	0.000043	0.512298	0.000039	0.512230	−2.76	0.76	0.80	1.22
	3-3-5	0.000017	0.000006	0.705518	0.000050	0.705518	0.048323	0.000019	0.512293	0.000037	0.512227	−2.82	0.72	0.79	1.22
Granite-gneiss-hosted vein type (late)	5602-1-1	0.001165	0.000290	0.706530	0.000970	0.706527	0.058093	0.000059	0.512069	0.000035	0.511990	−7.44	0.68	1.06	1.60
	5602-1-2	0.000059	0.000250	0.710192	0.000980	0.710192	0.055278	0.000071	0.512164	0.000047	0.512090	−5.51	0.92	0.95	1.44
	5602-1-3	0.000591	0.000310	0.710676	0.001100	0.710674	0.058374	0.000046	0.512115	0.000033	0.512036	−6.56	0.64	1.02	1.53
	~~5602-1-4~~	~~0.000185~~	~~0.000190~~	~~0.704796~~	~~0.000640~~	~~0.704796~~	~~0.043909~~	~~0.000140~~	~~0.511851~~	~~0.000180~~	~~0.511792~~	~~−11.32~~	~~3.51~~	~~1.17~~	~~1.92~~
	5602-1-5	0.000938	0.000260	0.708507	0.000770	0.708504	0.057200	0.000030	0.512139	0.000034	0.512061	−6.06	0.66	0.99	1.49
	5602-1-6	0.000343	0.000110	0.711396	0.000450	0.711395	0.059028	0.000047	0.512090	0.000030	0.512010	−7.05	0.58	1.04	1.57

Note: Initial $^{87}Sr/^{86}Sr$, $^{143}Nd/^{144}Nd$ values were calculated with age of 207 Ma in this study. The $\varepsilon_{Nd}(t)$ values are calculated based on present-day ($^{147}Sm/^{143}Nd)_{CHUR} = 0.1967$ and ($^{143}Nd/^{144}Nd)_{CHUR} = 0.512638$. Data with strikeout lines are not included in the figure due to its large error.

and Nd (>60000 ppm), which makes it relatively immune to crustal contamination (Bell and Blenkinsop, 1989). Therefore, a direct Sr-Nd isotopic study of monazite is an effective way to trace the sources of ore-forming materials.

In this study, in-situ Sr and Nd isotopic compositions of monazite were analyzed on thin sections where monazite coexists with betafite and carbonatitic calcite. As shown in Fig. 6, the Sr-Nd isotopic data of carbonatite-hosted and carbonatite-neared vein-type monazite is tightly distributed, similar to the carbonatite field with EM1-type mantle characteristics, except for those of granite-gneiss-hosted vein-type monazite with similar Nd but relatively higher Sr isotopic composition. This was also documented by the variation in Sr but relatively constant Nd isotopic compositions in calcite (Gao et al., 2021). This isotopic variation can be attributed to the fact that Sr ratios is less robust than those of Nd (Wall and Zaitsev, 2004). The greater changes in the Sr isotopic composition of granite-gneiss-hosted vein-type monazite (Sr-poor system) may be ascribed to either the mixing of Sr-rich and Nd-poor surrounding rocks, the alteration of later Sr-rich and Nd-poor crust-derived hydrothermal fluids, or both. In addition, monazites from multi-type ores (including monazites from both biotite plagioclase gneiss-hosted and granitic gneiss-hosted vein-type ores) display REE distribution patterns similar to those of typical carbonatite-related REE deposits (Fig. 5), which also supports genetically carbonatite-derived ortho-magmatic fluids.

These similarly integrated signatures (REE pattern and isotopic composition) convincingly indicate a close genetic relationship between the Huayangchuan REE-Nb-U mineralization and the EM1 mantle-derived carbonatite magma; that is, the REE-Nb-U ore-forming hydrothermal fluids are mainly from the carbonatite magma itself, rather than from the significant addition of external fluids.

6.3. Monazite mineral chemistry reveals higher HREE enrichment in late-stage mineralization

Monazite is one of the most important LREE minerals in carbonatite-related deposits and develops from the early to late stages of mineralization; accordingly, monazite can be used to trace the evolutionary processes of ore-forming fluids. As shown in Fig. 7, the strong correlation of REY + P and Th + Si + Ca (Fig. 7a) of the monazite is likely due to the huttonite- and cheralite-related solid solutions that result from the following coupled substitution processes (Gramaccioli and Segalstad, 1978; van Emden et al., 1997):

$REY^{3+}+P^{5+} \leftrightarrow Th^{4+}+Si^{4+}$ and $2REY^{3+} \leftrightarrow Ca^{2+}+Th^{4+}$.

The monazite sampled in our study contains minor S content (up to 0.81 wt%, Table S1), and there is a correlation between P and S (Fig. 7b) but no obvious correlation between S and F (Fig. 7c), indicating the coupled substitutions of $P^{5+}+REY^{3+} \leftrightarrow S^{6+} + Ca^{2+}$ (Wall and Zaitsev, 2004). The decreasing trend of S content from early carbonatite-hosted monazite to late vein-type monazite (Fig. 7b) may be ascribed to the participation of barytocelestite (Fig. 3c), which is indicative of decreased sulfur fugacity during the evolution of ore-forming fluids. The strong correlation between As and Nd (Fig. 7d) can be ascribed to the presence of AsO_4^{3-}, which substitutes PO_4^{3-} in the monazite lattice (Clavier and Dacheux, 2011). The diagram of V vs. As shows that in the carbonatite system, the content of V presents a changing trend from 50 to 300 ppm, but As remains constant at ca. 250 ppm (Fig. 7e). In the late hydrothermal veins, As increased, while V continued to decrease. The strong linear correlation between V and As may be indicative of the mechanism of substitution (Fig. 7e).

Overall, different types of monazites show similar REE patterns (Fig. 5) and total LREE contents, but significantly different MREE and HREE contents, showing an obvious increasing trend from early carbonatite-hosted ore to late hydrothermal vein-type ore (distant from carbonatite) (Fig. 7f). This late monazite ΣHREE enrichment trend exists not only at Huayangchuan but also in the Djupedal hydrothermal REE deposit (Fig. 7f). Individual REEs usually show different variation

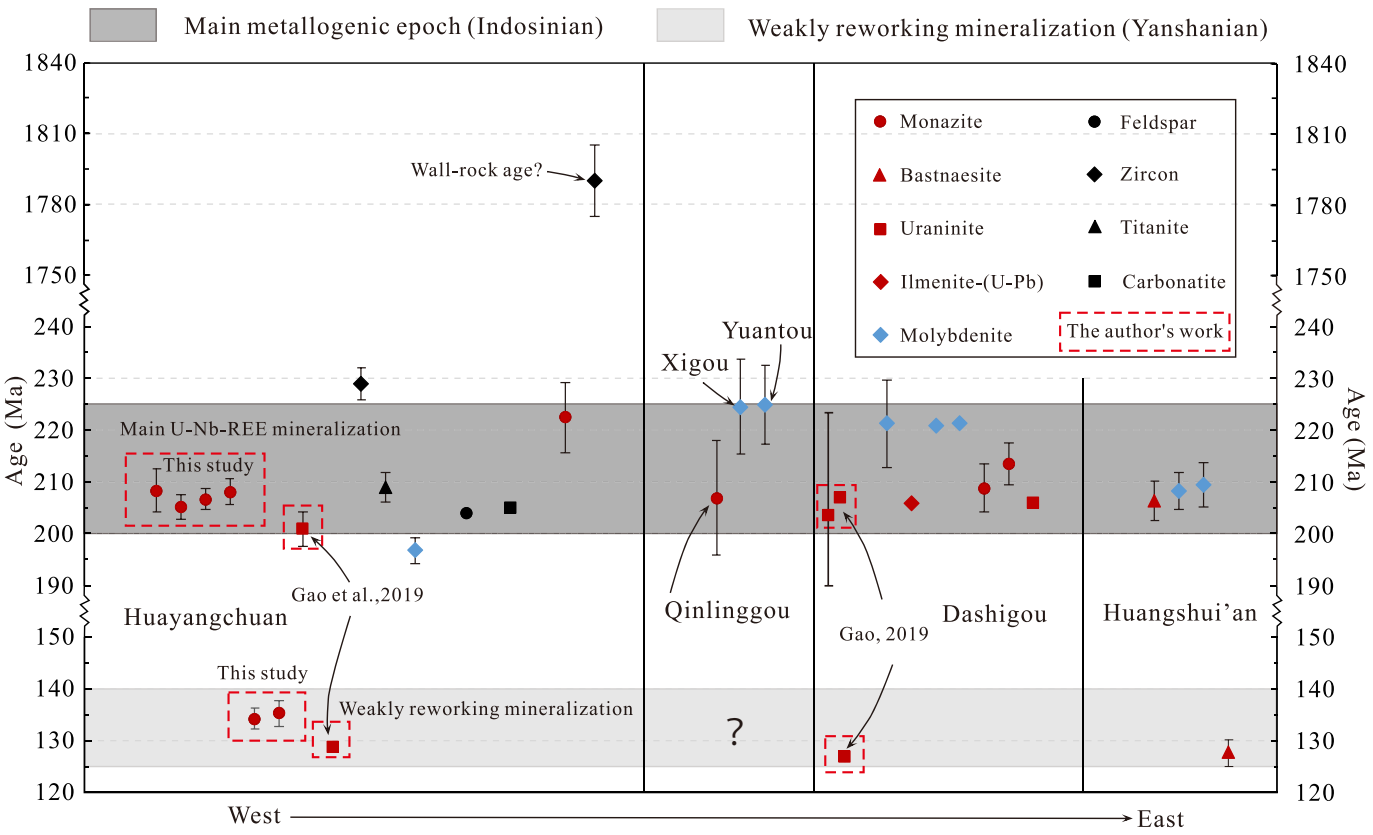

Fig. 9. Age spectra of Late Triassic carbonatitic magmatism (including late Cretaceous thermal events) and the associated (H)REE-Nb-U-Mo polymetallic mineralization in the Lesser Qinling. References: Huayangchuan (Qiu et al., 1993; Gao et al., 2019; Jiang et al., 2020; Wang et al., 2020; Xue et al., 2020; Zheng et al., 2020a); Xigou (Du et al., 2020); Qinlinggou (Wang et al., 2020); Yuantou (Song et al., 2015); Dashigou (Huang et al., 1984, 1994; Stein et al., 1997; Song et al., 2016; Gao, 2019; Wang et al., 2020); Huangshui'an (Huang et al., 2009; Cao et al., 2014; Zhang et al., 2019; She et al., 2022). The detailed chronological data and their sources of rare polymetallic deposits are presented in Table S3.

trends, such as a significantly decreasing trend for La, but Ce remains constant from early carbonatite-hosted monazite to late vein-type monazite (Fig. 8a-c), showing a tight pivot round Ce (Fig. 5), as reported by Wall and Zaitsev (2004). This may reflect different sector growth that favors the absorption of either La or smaller Pr and Nd cations (Cressey et al., 1999; Wall and Zaitsev, 2004). Interestingly, in diagrams of Sm vs. Eu, Gd vs. Tb, Ho vs. Er, Dy vs. Y, and Yb vs. Lu (Fig. 8e–i), most of these MREE and HREE of multi-type monazites from the Huayangchuan deposit show a synergistic increasing trend from early carbonatite-hosted monazite to late vein-type monazite, except for low contents of Yb and Lu (Fig. 8i). The relatively HREE- and/or MREE-rich features of late-stage monazite and calcite compared with early carbonatite-hosted monazite or igneous calcite (for the enrichment of MREE and HREE in calcite, see Gao et al., 2021) indicate that MREE and HREE may be more likely to dissolve in magmas or fluids for long-distance migration than LREE.

In fact, a similar rule has also been verified by the exploration of the Bayan Obo carbonatite-related LREE-dominated deposit in recent years; that is, there are, indeed, different degrees of HREE mineral enrichment in locally peripheral parts of the ore district (fergusonite-Y, Zhang and Tao, 1987; Gong, 1991; Liu et al., 2020). From the early skarn stage to the late Na-K-(F) metasomatic stage, chemical and evolutionary studies of fergusonite-group minerals show a decreasing trend of LREE (La, Ce, Pr, Sm) but an increasing trend of MREE and HREE (Gd, Tb, Ho, Lu, Y) (Gong, 1991), suggesting that MREE and HREE tend to be enriched in the late hydrothermal ore-forming fluids. Furthermore, similar HREE-rich trends also appear in the Songwe Hill (Malawi), Tarim, and Huayangchuan (China) carbonatite systems, that is, the late apatite shows a high HREE-rich feature, accompanied by a certain amount of xenotime mineralization (Broom-Fendley et al., 2017), and by increasing the HREE/LREE ratio for the whole rock (Song et al., 2020) and corresponding magmatic calcite in the late calcite carbonatites during the evolution of carbonate magma (Gao et al., 2021).

In addition to the carbonatite systems, similar late monazite ΣHREE enrichment trends have also been observed in some other REE hydrothermal systems. Andersson et al. (2018) concluded that the Djupedal deposit is a hydrothermal REE-phosphate deposit with HREE-rich monazite as the main REE mineral. On the basis of the restricted set of their monazite data used in the present study, we found that the late vein-type monazite (ΣHREE: 37525–55705 ppm; mean value: 49262 ppm, n = 9) displays higher HREE content than the early primary Djupedal monazite (ΣHREE: 34238–42368 ppm; mean value: 38667 ppm, n = 5) (Fig. 8f-i), although the other individual REE variation trends are not completely similar to those of the Huayangchuan monazite (Fig. 8b-e). These cases imply that HREE may tend to be enriched in late ore-forming fluids during the evolution of carbonatite and some other hydrothermal systems.

6.4. *HREE-rich mechanisms and its implications for HREE mineralization*

The results of our study—combined with previous findings—shed some light on why the late ore-forming fluids or carbonatitic magma have an HREE-rich trend in some LREE-rich systems. Two important factors may be responsible for this: systems with abundant HREE may be related to an HREE-rich source, or it may be controlled by the differences in the geochemical behavior of LREE and HREE during the evolution of ore-forming hydrothermal fluids. Previous studies have shown that the HREE-rich carbonatites in the Lesser Qinling may be related to

an HREE-rich source, and the high evolution process further promoted the enrichment of HREE in the late carbonatitic magma, prioritizing intense carbonatite-exsolved ore-forming fluids associated with intense fenitization (Gao et al., 2021). Therefore, carbonatites formed in this situation, such as the Huayangchuan and Dashigou carbonatites in the Lesser Qinling, may have high potential for HREE mineralization. In addition, it has been reported that carbonatitic magma with considerable REE mineralization generally undergoes a complete evolutionary process from the magmatic stage to the hydrothermal stage (Xie et al., 2009; Yang et al., 2019). During this process, carbonatite-exsolved ore-forming fluids often react with wall rocks, thus developing extensive sodic fenitization (earlier, higher temperature) and potassic fenitization (later, relatively lower temperature) (Le Bas, 2008). This is also consistent with observations from the Huayangchuan case that the carbonatite system evolved from the early Na-rich stage (Na-bearing calcite carbonatite and Na-rich aegirine-augite calcite carbonatite; Fig. 2a-b) to the late K-rich stage (biotite-bearing calcite carbonatite and K-fenite) (Fig. 2c-d). Interestingly, experimental geochemical studies have shown that both Na and K produce higher HREE/LREE ratios in the transported fluids, but K-rich fluids preferentially transport HREE relative to Na-rich fluids; thus, both LREE and HREE are expected in sodic fenite, but the highest HREE/LREE ratios are expected in potassic fenite (Anenburg et al., 2020). In the present study, late vein-type LREE-dominated monazite coexisting with biotite and K-feldspar (a K-rich hydrothermal system) displayed HREE-rich features. This may indicate that LREE are more likely to precipitate in the early stage than HREE, and HREE will be more dissolved, leading to a higher degree of transportation and enrichment in the late ore-forming fluids with the evolution of ore-forming fluids. As discussed above, HREE and MREE may be more likely to dissolve in hydrothermal fluids (resulting in long-distance migration). However, the migration distance of MREE and HREE may depend on the tectonic setting of carbonatites. Some case studies of carbonatite-related REE deposits from orogenic tectonic settings show that REE mineralization mainly occurs in or immediately surrounding the causative carbonatite, and that vein-type REE mineralization is not very far from the carbonatite (Xie et al., 2016, 2019). In such settings, carbonatites usually occur as tiny veined lenses (Yang and Yang, 1998) and the carbonatite-related vein-type REE mineralization is confined to a limited fault system, such as the Maoniuping deposit (Xie et al., 2016) and the Huayangchuan case in this study. However, the tectonic setting of mineralized carbonatites is varied. For some carbonatite systems from the rift setting (e.g., East African Continent Rift), the width of fenitised aureoles can be up to 1 km (Chilwa Island carbonatite complex; Dowman et al., 2017), and REE fractionation occurs during long-distance migration in such systems, resulting in HREE enrichment in late-stage apatite associated with minor xenotime-Y mineralization (Broom-Fendley et al., 2017). In the present study, we determined that, although late vein-type REE mineralization did not migrate far, the tendency of HREE to be further enriched in late vein-type ores is evident by the change trend of the chemical composition of LREE-dominated monazite (Fig. 8). Thus, we suggest that the trend of HREE enrichment in monazite may as one of the indicators for the HREE exploration in some potential area. In addition to monazite, multi-stage igneous calcites of the main part of the Huayangchuan unmineralized calcite carbonatite display an HREE enrichment trend from early coarse-grained calcite (Cal-I-1, av. 472 ppm) to late fine-grained calcite (Cal-I-3, up to 774 ppm, av. 721 ppm) before carbonatite-exsolved ore-forming fluid (Fig. 10, Gao et al., 2021). For mineralized calcite carbonatite (associated with REE-Nb-U mineralization), although HREE contents decrease from early calcite (Cal-I-1, av. 472 ppm) to late calcite (Cal-I-3, av. 280 ppm)(Fig. 10), the locally HREE-saturated precipitation of minor HREE-rich fergusonite-Y associated with late calcite (Cal-I-3), betafite and monazite (Gao et al., 2021) further indicates an HREE enrichment trend in the late stage of the carbonatite-related system (Fig. 10). Therefore, a certain degree of HREE enrichment potential may be expected in the periphery (possibly potassic fenitization zone) of some large carbonatite-related LREE-dominated deposits accompanied by extensive exsolving of REE-rich fluids, which is supported by some case studies (Gong, 1991; Broom-Fendley et al., 2021), but further integrated studies on the HREE enrichment law of whole rocks or various minerals are needed in more typical cases.

7. Conclusions

(1) SIMS U-Pb dating of in-situ monazites yielded an initial age of 207 Ma and some younger reworking ages, indicating that the Huayangchuan REE-Nb-U deposit mainly formed in the Late Triassic but was overprinted by Yanshanian magmatism. Such a weak reworking process not only occurs in the Huayangchuan, but also widely exists in other carbonatite-related deposits in the Lesser Qinling.

(2) The monazite Sr-Nd isotopic compositions support the idea that REE-Nb-U ore-forming materials of the Huayangchuan deposit are genetically related to EM1 mantle-derived calcite carbonatite.

(3) The trace element characteristics of monazites reveal that HREE may be more likely to dissolve in fluids for long-distance migration than LREE during the carbonatite-exsolved ore-forming fluids, indicating a certain HREE enrichment and mineralization potential may in the periphery of some large carbonatite-related LREE-dominated deposits accompanied by extensive exsolving REE-rich fluids.

(4) Late Triassic carbonatites in the Lesser Qinling are not only important for rare metal mineralization (LREE ± Nb ± U ± Mo) but also for more valuable HREE mineralization potential.

Declaration of Competing Interest

The authors declare that they have no known competing financial

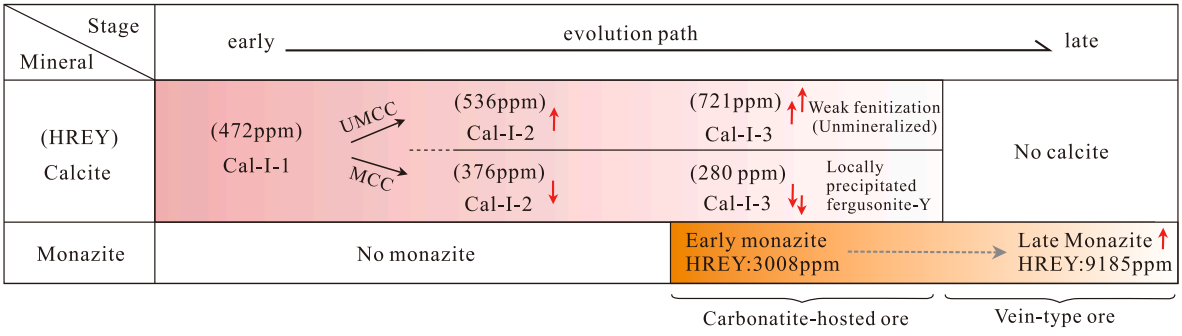

Fig. 10. Late HREE enrichment trend recorded by multi-stage calcites and monazites in the Huayangchuan carbonatite-related system. The content of HREY is given as an average value. Calcite classification and data source: Gao et al. (2021). Abbreviation: UMCC, unmineralized calcite carbonatite; MCC, mineralized calcite carbonatite.

interests or personal relationships that could have appeared to influence the work reported in this paper.

Data availability

Data will be made available on request.

Acknowledgements

This research is financially supported by the Strategic Priority Research Program (B) of Chinese Academy of Sciences (Grant No. XDB18030200) and the National Natural Science Foundation of China (Grant Nos. 41473049 and 41103027). Thanks to Dr. Cheng Gao and Qing-Qing Kang senior engineer from the Geological Team 224 Sino Shaanxi Nuclear Industry Group for their help in the field geology work at Huayangchuan. Drs. Xiang Li, and Yan-Wen Tang are kindly thanked for performing in-situ major and trace element analyses on monazite for this paper, respectively. Thanks to Yu Liu, Guo-Qiang Tang, Xiao-Xiao Ling senior engineers and Jiao Li senior experimentalist for their helping with SIMS monazite U-Pb dating. Thanks to Ms. Hong-Xia Ma for her help on specimen preparation. The authors would also like to thank the editor, and the anonymous reviewers for their helpful comments and constructive suggestions to have improved the quality of this paper.

Appendix A. Supplementary data

Supplementary data to this article can be found online at https://doi.org/10.1016/j.oregeorev.2023.105450.

References

Aleinikoff, J.N., Schenck, W.S., Plank, M.O., Srogi, L., Fanning, C.M., Kamo, S.L., Bosbyshell, H., 2006. Deciphering igneous and metamorphic events in high-grade rocks of the Wilmington complex, Delaware: morphology, cathodoluminescence and backscattered electron zoning, and SHRIMP U-Pb geochronology of zircon and monazite. Geol. Soc. Am. Bull. 118, 39–64.

Andersson, S.S., Wagner, T., Jonsson, E., Michallik, R.M., 2018. Mineralogy, paragenesis, and mineral chemistry of REEs in the Olserum-Djupedal REE-phosphate mineralization, SE Sweden. Am. Miner. 103, 125–142.

Anenburg, M., Mavrogenes, J., Frigo, C., Wall, F., 2020. Rare earth element mobility in and around carbonatites controlled by sodium, potassium, and silica. Sci. Adv. 6, 1–10.

Bai, T., Chen, W., Jiang, S.Y., 2019. Evolution of the carbonatite Mo-HREE deposits in the Lesser Qinling Orogen: Insights from in situ geochemical investigation of calcite and sulfate. Ore Geol. Rev. 113, 103069.

Bell, K., Blenkinsop, J., 1989. Neodymium and strontium isotope geochemistry of carbonatites. In: Bell, K. (Ed.), Carbonatites: genesis and evolution. Unwin Hyman, London, pp. 278–300.

British Geological Survey, 2011. Rare earth elements, 1–53.

Broom-Fendley, S., Brady, A.E., Wall, F., Gunn, G., Dawes, W., 2017. REE minerals at the Songwe Hill carbonatite, Malawi: HREE-enrichment in late-stage apatite. Ore Geol. Rev. 81, 23–41.

Broom-Fendley, S., Smith, M., Andrade, M., Ray, S., Banks, D., Loye, E., Atencio, D., Pickles, J., Wall, F., 2019. Sulfur-bearing monazite-(Ce) from the Eureka carbonatite, Namibia: oxidation state, substitution mechanism, and formation conditions. Mineral Mag. 1–44.

Broom-Fendley, S., Elliott, H.A.L., Beard, C.D., Wall, F., Armitage, P.E.B., Brady, A.E., Deady, E., Dawes, W., 2021. Enrichment of heavy REE and Th in carbonatite-derived fenite breccia. Geol. Mag. 1–17.

Budzyń, B., Wirth, R., Sláma, J., Birski, Ł., Tramm, F., Kozub-Budzyń, G., et al., 2021. LA-ICPMS, TEM and Raman study of radiation damage, fluid-induced alteration and disturbance of U-Pb and Th-Pb ages in experimentally metasomatised monazite. Chem. Geol. 583, 120464.

Cai, J., Yu. L., Xu, D., Gao, C., Chen, G., Yu, D., Jiao, Q., Ye, T., Zou, S., Li, L., 2020. Multiple episodes of tectono-thermal disturbances in the Huayangchuan U-Nb-Pb polymetallic deposit in the Xiaoqinling region, central China and their significances on metallogeny. Ore Geol. Rev. 103755.

Cao, M., Qin, K., Evans, N.J., Li, G., Ling, X., McInnes, B.I.A., Zhao, J.X., 2021. Titanite in situ SIMS U-Pb geochronology, elemental and Nd isotopic signatures record mineralization and fluid characteristics at the Pusangguo skarn deposit. Tibet. Miner. Depos. 56, 907–916.

Cao, J., Ye, H.S., Li, H.Y., Li, Z.Y., Zhang, X.K., He, W., Li, C., 2014. Geological characteristics and molybdenite Re-Os isotopic dating of Huangshuian carbonatite vein-type Mo (Pb)deposit in Songxian County, Henan Province. Mineral Deposits 33, 53–69 in Chinese with English abstract.

Cherniak, D.J., Watson, E.B., Grove, M., Harrison, T.M., 2004. Pb diffusion in monazite: a combined RBS/SIMS study. Geochim. Cosmochim. Acta 68, 829–840.

Chi, R.A., Tian, J., 2007. Review of weathered crust rare earth ore. J. Chin. Rare Earth Soc. 25, 641–650 in Chinese with English abstract.

Clavier, N., Dacheux, N., 2011. Crystal chemistry of the monazite structure. J. Eur. Ceram. Soc. 31, 941–976.

Cressey, G., Wall, F., Cressey, B.A., 1999. Differential REE uptake by sector growth of monazite. Mineral Mag. 63 (6), 813–828.

Dobson, D.P., Jones, A.P., Rabe, R., Sekine, T., Kurita, K., Taniguchi, T., Kondo, T., Kato, T., Shimomura, O., Urakawa, S., 1996. In-situ measurement of viscosity and density of carbonate melts at high pressure. Earth Planet. Sci. Lett. 143, 207–215.

Dowman, E., Wall, F., Treloar, P.J., Rankin, A.H., 2017. Rare-earth mobility as a result of multiple phases of fluid activity in fenite around the Chilwa Island Carbonatite. Malawi. Mineral Mag. 81, 1367–1395.

Du, Z.W., Ye, H.S., Mao, J.W., Meng, F., Cao, J., Wang, P., Wei, Z., Ding, J.H., 2020. Molybdenite Re-Os gochronology and isotope geochemical characteristics of Xigou molybdenum deposit in Shaanxi Province and its geological significance. Miner. Depos. 39, 728–744 in Chinese with English abstract.

Gao, L.G., Chen, Y.W., Bi, X.W., Hu, R.Z., Gao, C., Dong, S.H., Luo, J.C., 2019. Chronology and mineral chemistry of the uranium minerals in Huayangchuan uranium-niobium deposit, Shaanxi Province and itsimplications for uranium mineralization. Acta Geol. Sin. 93, 2273–2291 in Chinese with English abstract.

Gao, L.G., Chen, Y.W., Bi, X.W., Gao, J.F., Chen, W.T., Dong, S.H., Luo, J.C., 2021. Genesis of carbonatite and associated U-Nb-REE mineralization at Huayangchuan, Central China: Insights from mineral paragenesis, chemical and Sr-Nd-C-O isotopic compositons of calcite. Ore Geol. Rev. 138, 10431.

Gao, C., Kang, Q.Q., Jiang, H.J., Zheng, H., Li, P., Zhang, X.M., Li, L., Dong, Q.Q., Ye, X. C., Hu, X.J., 2017. A unique uranium polymetallic deposit discovered in the Qinling orogenic belt: The Huayangchuan super-large U-Nb-Pb-REE deposit associated with pegmatites and carbonatites. Geochimica 46, 446–455 in Chinese with English abstract.

Gao, X.Y., Zhao, T.P., Chen, W.T., 2014. Petrogenesis of the early Cretaceous Funiushan granites on the southern margin of the North China Craton: implications for the Mesozoic geological evolution. J. Asian Earth Sci. 94, 28–44.

Gao, J.F., Zhou, M.F., 2013. Generation and evolution of siliceous high magnesium basaltic magmas in the formation of the Permian Huangshandong intrusion (Xinjiang, NW China). Lithos 162, 128–139.

Gao, L.G., 2019. Uranium-niobium polymetallic deposits related to carbonatite rocks in the Qinling, China: case studies of the Huayangchuan and Dashigou deposits. Master dissertation. University of Chinese Academy of Sciences, 1-115 (in Chinese with English abstract).

Genge, M.J., Price, G.D., Jones, A.P., 1995. Molecular dynamics simulations of $CaCO_3$ melts to mantle pressures and temperatures: implications for carbonatite magmas. Earth and Planetary Science Letters 131, 225–238.

Gong, W.L., 1991. Chemistry and evolution of fergusonite-group minerals, Bayan Obo, inner Mongolia. Chin. J. Geochem. 10, 266–276.

Goodenough, K., Wall, F., Merriman, D., 2018. The rare earth elements: demand, global resources, and challenges for resourcing future generations. Nat. Resour. Res. 27 (2), 201–216.

Gramaccioli, C.M., Segalstad, T., 1978. A uranium- and thorium-rich monazite from a south-Alpine pegmatite at Piona, Italy. Am. Mineral. 63, 757–761.

Guo, B., Zhu, L.M., Li, B., Gong, H.J., Wang, J.Q., 2009. Zicron U-Pb age and Hf isotope composition of the Huashan and Heyu granite plutons at the southern margion of North China Craton: Implications for geodynamic settings. Acta. Petrol. Sin. 25, 265–281 in Chinese with English abstract.

Henderson, P., 1984. Rare earth element geochemistry. Elsevier, Amsterdam, pp. 1–510.

Hodell, D.A., Mead, G.A., Mueller, P.A., 1990. Variation in the strontium isotopic composition of seawater (8 Ma to present): Implications for chemical weathering rates and dissolved fluxes to the oceans. Chem. Geol. 80, 291–307.

Huang, D.H., Wang, Y.C., Nie, F.J., Jiang, X.J., 1984. Isotopic composition of sulfur, carboon and oxygen and source of the Huanglongpu carbonatite vein-type of molybdenum (lead) deposits. Acta Geol. Sin. 3, 252–264 in Chinese with English abstract.

Huang, D.H., Wu, C.Y., Du, A.D., He, H.L., 1994. Re-Os isotope ages of molybdenum deposits in east qinling and their significance. Miner. Depos. 13, 221–230 in Chinese with English abstract.

Huang, D.H., Hou, Z.Q., Yang, Z.M., Li, Z.Q., Xu, D.X., 2009. Geological and geochemical characteristics, metallogenetic mechanism and tectonic setting of carbonatite vein-type Mo (Pb) deposits in the East Qinling molybdenum ore belt. Acta Geol. Sin. 83, 1968–1984 in Chinese with English abstract.

Isnard, H., Brennetot, R., Caussignac, C., Caussignac, N., Chartier, F., 2005. Investigations for determination of Gd and Sm isotopic compositions in spent nuclear fuels samples by MC-ICPMS. Int. J. Mass Spectrom. 246, 66–73.

Jiang, H.J., Gao, C., Kang, Q.Q., Chen, H.Y., Zheng, H., Chen, B., Dong, Q.Q., Zhang, X. M., Li, P., Li, L., Liu, K.H., He, S.P., 2020. Mineralization paragenesis of Huayangchuan U-Nb-Pb deposit in the Lesser Qinling. Geotect. Metall. 44, 404–421 in Chinese with English abstract.

Kang, Q.Q., Jiang, H.J., Li, P., Zhang, X.M., Dong, Q.Q., Ye, X.C., Gao, C., Zhang, T., Xue, C.C., 2018. Ore mineralogical characteristics of the Huayangchuan U-Nb-Pb deposit. J. East. China Univ. Technol. 41, 111–123 in Chinese with English abstract.

Keppler, H., 2003. Water solubility in carbonatite melts. Am Miner 88, 1822–1824.

Le Bas, M.J., 2008. Fenites associated with carbonatites. Canmin. Mineral. 46, 915–932.

Li, N., Chen, Y.J., Fletcher, I.R., Zeng, Q.T., 2011. Triassic mineralization with Cretaceous overprint in the Dahu Au-Mo deposit, Xiaoqinling gold province: Constraints from SHRIMP monazite U-Th-Pb geochronology. Gondwana Res. 20, 543–552.

Li, Q.L., Li, X.H., Lan, Z.W., Guo, C.L., Yang, Y.N., Liu, Y., Tang, G.Q., 2013. Monazite and xenotime U-Th-Pb geochronology by ion microprobe: dating highly fractionated granites at Xihuashan tungsten mine, SE China. Contrib. Mineral. Petrol. 166, 65–80.
Li, X.C., Yang, K.F., Spandler, C., Fan, H.R., Zhou, M.F., Hao, J.L., et al., 2021. The effect of fluid-aided modification on the Sm-Nd and Th-Pb geochronology of monazite and bastnäsite: Implication for resolving complex isotopic age data in REE ore systems. Geochim. Cosmochim. Acta 300, 1–24.
Ling, X.X., Huyskens, M.H., Li, Q.L., Yin, Q.Z., Werner, R., Liu, Y., Tang, G.Q., Yang, Y.N., Li, X.H., 2017. Monazite RW-1: a homogenous natural reference material for SIMS U-Pb and Th-Pb isotopic analysis. Mineral Petrol. 111, 163–172.
Liu, S., Ding, L., Fan, H.R., Yang, K.F., Tang, Y.W., She, H.D., Hao, M.Z., 2020. Hydrothermal genesis of Nb mineralization in the giant Bayan Obo REE-Nb-Fe deposit (China): Implicated by petrography and geochemistry of Nb-bearing minerals. Precambr. Res. 348, 105864.
Liu, Z., Li, C., Jia, X., Li, G., Qiang, L., Ma, J., et al., 2021. Study on comprehensive recovery technology of Huayangchuan low grade U-Nb-Pb polymetallic ore. Conserv. Util. Miner. Resour. 3, 132–137.
Ludwig, K.R., 2003. User's manual for Isoplot 3.00: a geochronological toolkit forMicrosoft Excel. Berkeley Geochronology Center Special Publication 4, 71.
Ma, L., Qiao, X., Liu, N., et al., 2002. Geological atlas of China. Geol. Publ. House, Beijing, pp. 1–348 (in Chinese).
McDonough, W.F., Sun, S.S., 1995. The composition of the Earth. Chem. Geol. 120, 223–253.
Meng, Q.R., Zhang, G.W., 1999. Timing of collision of the North and South China blocks: Controversy and reconciliation. Geology 27, 123–126.
Meng, Q.R., Zhang, G.W., 2000. Geologic framework and tectonic evolution of the Qinling orogen, central China. Tectonophysics 323, 183–196.
Qiu, J.X., Zeng, G.C., Li, C.N., 1993. Alkaline igneous rocks in Qinling-Daba Mountains. Geol. Publ. House, Beijing, pp 1-183 (in Chinese).
Ramos, F.C., Wolff, J.A., Tollstrup, D.L., 2004. Measuring $^{87}Sr/^{86}Sr$ variations in minerals and groundmass from basalts using LA-MC-ICPMS. Chem. Geol. 211, 135–158.
She, H.D., Fan, H.R., Yang, K.F., Li, X.H., Wang, Z.Y., 2022. REEs upgrading by post-carbonatite fluids in the Huangshui'an Mo-REE deposit, eastern Qinling Orogen (central China). Ore Geol. Rev. 150, 105177.
Smith, M., Kynicky, J., Xu, C., Song, W., Spratt, J., Jeffries, T., Brtnicky, M., Kopriva, A., Cangelosi, D., 2018. The origin of secondary heavy rare earth element enrichment in carbonatites: Constraints from the evolution of the Huanglongpu district, China. Lithos 308–309, 65–82.
Song, W.L., Xu, C., Kynicky, J., 2020. Heavy rare earth element (HREE) enrichment in carbonatites: A case study from a xenotime-bearing carbonatite REE deposit in Bachu, Xinjiang of China. Goldschmidt Abstract. p. 2436.
Song, W.L., Xu, C., Qi, L., Zhou, L., Wang, L., Kynicky, J., 2015. Genesis of Si-rich carbonatites in Huanglongpu Mo deposit, Lesser Qinling orogen, China and significance for Mo mineralization. Ore Geol. Rev. 64, 756–765.
Song, W.L., Xu, C., Smith, M.P., Kynicky, J., Huang, K., Wei, C., Zhou, L., Shu, Q., 2016. Origin of unusual HREE-Mo-rich carbonatites in the Qinling orogeny, China. Sci. Rep. 6, 1–10.
Stein, H.J., Markey, R.J., Morgan, J.W., 1997. Highly precise and accurate Re-Os ages for molybdenite from the East Qinling molybdenum belt, Shaanxi Province, China. Economic Geology 92, 827–835.
van Emden, B., Thornber, M.R., Graham, J., Lincoln, F., 1997. The incorporation of actinides in monazite and xenotime from placer deposits in Western Australia. Can. Mineral. 35, 95–104.
Wall, F., Zaitsev, A.N., 2004. Rare earth minerals in Kola carbonatites. In: Wall, F., Zaitsev, A.N. (Eds.), Phoscorites and carbonatites from mantle to mine: the key example of the Kola alkaline province. Mineralogical Society of Great Britain and Ireland, pp. 341–374.
Wang, J.Y., Li, Z.D., Zhang, Q., Li, C., Xie, Y., Li, G.Y., Zeng, W., Ding, N., 2020. Metallogenic epoch of the carbonatite-type Mo-U polymetallic deposit in east Qinling:evidence from the monazite LA-ICP-MS U-Pb and molybdenite Re-Os isotopic dating. Acta Geol. Sin. 94, 2946–2964.
Woolley, A.R., Kjarsgaard, B.A., 2008. Carbonatite occurrences of the world: Map and database. Geol. Survey Canada open file report 5796.
Xie, Y.L., Hou, Z.Q., Yin, S.P., Dominy, S.C., Xu, J.H., Tian, S.H., Xu, W.Y., 2009. Continuous carbonatitic melt–fluid evolution of a REE mineralization system: Evidence from inclusions in the Maoniuping REE Deposit, Western Sichuan. China. Ore Geol. Rev. 36, 90–105.
Xie, Y.L., Hou, Z.Q., Goldfarb, R., Guo, X., Wang, L., 2016. Rare Earth Element Deposits in China. Rev. Econ. Geol. 18, 115–136.
Xie, Y.L., Verplanck, P., Hou, Z.Q., Zhong, R., 2019. Rare Earth Element Deposits in China: a review and some new understanding. Soc. Econ. Geol. Spec. Publ. 22, 509–552.
Xu, C., Campbell, I.H., Allen, C.M., Huang, Z., Qi, L., Zhang, H., Zhang, G., 2007. Flat rare earth element patterns as an indicator of cumulate processes in the Lesser Qinling carbonatites, China. Lithos 95, 267–278.
Xu, C., Taylor, R.N., Kynicky, J., Chakhmouradian, A.R., Song, W., Wang, L., 2011. The origin of enriched mantle beneath North China block: Evidence from young carbonatites. Lithos 127, 1–9.
Xue, S., Ling, M.X., Liu, Y.L., Kang, Q.Q., Huang, R.F., Zhang, Z.K., Sun, W.D., 2020. The formation of the giant Huayangchuan U-Nb deposit associated with carbonatite in the Qinling Orogenic Belt. Ore Geol. Rev. 122, 103498.
Yang, K.F., Fan, H.R., Pirajno, F., Li, X.C., 2019. The Bayan Obo (China) giant REE accumulation conundrum elucidated by intense magmatic differentiation of carbonatite. Geology 47, 1198–1202.
Yang, Y.H., Wu, F.Y., Yang, J.H., Chew, D.M., Xie, L.W., Chu, Z.Y., Zhang, Y.B., Huang, C., 2014. Sr and Nd isotopic compositions of apatite reference materials used in U-Th-Pb geochronology. Chem. Geol. 385, 35–55.
Yang, X.M., Yang, X.Y., 1998. Carbonatite: a probe rock for the tectonic settings of continental lithosphere and mantle metasomatism. Chin. J. Geophys. 41 (S), 228–235.
Zhang, W., Chen, W.T., Gao, J.F., Chen, H.K., Li, J.H., 2019. Two episodes of REE mineralization in the Qinling Orogenic Belt, Central China: in-situ U-Th-Pb dating of bastnäsite and monazite. Miner. Depos. 54, 1265–1280.
Zhang, P.S., Tao, K.J., 1987. Charcteristics of the fergusonite group and aeschynite group minerals in China. J. Chin. Rare Earth Soc. 1, 1–7 in Chinese with English abstract.
Zhang, X.K., Ye, H.S., Li, Z.Y., Cao, J., Wang, X.Y., 2015. Zircon U-Pb ages, Hf isotopic composition and geochemistry of Dafuyu granitoid poluton from Huashan complex batholith in Xiaoqinling. Miner. Depos. 34, 235–260 in Chinese with English abstract.
Zheng, H., Chen, H., Li, D., Wu, C., Chen, X., Lai, C.K., 2020a. Timing of carbonatite-hosted U-polymetallic mineralization in the supergiant Huayangchuan deposit, Qinling Orogen: Constraints from titanite U-Pb and molybdenite Re-Os dating. Geosci. Front. 11, 1581–1592.
Zheng, H., Chen, H.Y., Wu, C., Jiang, H.J., Gao, C., Kang, Q.Q., Yang, C.S., Wang, D.Q., Lai, C.K., 2020b. Genesis of the supergiant Huayangchuan carbonatite-hosted uranium-polymetallic deposit in the Qinling Orogen, Central China. Gondwana Res. 86, 250–265.
Zindler, A., Hart, S., 1986. Chemical geodynamics. Annu. Rev. Earth. Planet. Sci. 14, 493–571.